# Determining the Strong Coupling Constant using Lattice QCD

Matthew Inglis-Whalen

August 22, 2014


MSc in Theoretical Physics

The University of Edinburgh

2014

**Abstract**

A determination of $\alpha_{\overline{MS}}^{(n_f=5)}(m_Z)$ is presented using $n_f = 0$ and $n_f = 2$ lattice data taken from the literature. Closely following previous work by the QCDSF-UKQCD Collaboration, the main motivation for this paper is a newly determined value for the Sommer parameter $r_0$, as well as recently updated values of the inverse lattice spacing $r_0/a$. It is found that $\alpha_{\overline{MS}}^{(n_f=5)}(m_Z) = 0.1146 \pm 0.0016$, in tension with the current world average.

# Contents

# List of Tables

# List of Figures

I would like to thank Dr. Roger Horsley for our many talks throughout the summer. His experience was highly beneficial to my understanding of Lattice QCD, and his supervision key to the completion of this work within the short time frame.

*~ The devil's in the details ~*

# Chapter 1

# Introduction

## 1.1 Motivation

The quantum field theory describing the interactions of coloured particles, commonly known as Quantum Chromodynamics (QCD), is built from the requirement that the standard model (SM) Lagrangian density must be locally invariant under any $SU(3)$ transformation acting on quark field colour indices. The theory exhibits two important characteristics: asymptotic freedom and confinement. *Asymptotic freedom* is the qualitative observation that at high energies QCD becomes weakly coupled, allowing for accurate physical predictions through the use of perturbation theory. Conversely, *confinement* describes the observation that at low energies QCD becomes strongly coupled, which precludes the use of perturbation theory and thus requires a non-perturbative approach.

In energy regimes where perturbation theory applies, physical quantities are calculated by summing Feynman diagrams for the relevant process. The final result is expressed as a truncated series expansion in powers of the *strong coupling constant*, $\alpha_s$. Truncating the series at higher powers of $\alpha_s$ gives increasingly accurate results, with the stumbling block being that higher order terms in the series are exponentially more difficult to calculate. Yet even if the expansion coefficients were known to all orders, the degree of precision currently placed on $\alpha_s$ is not sufficient to justify keeping terms with more than 3 powers of $\alpha_s$ above leading order (NNNLO). The current world average for the strong coupling constant is [1]

$$\alpha_s(m_Z) = 0.1185 \pm 0.0006, \tag{1.1}$$

which means that even at the energy scale of the Z boson mass, where $\alpha_s$ is most precisely known, the NNNLO term is already of the same magnitude as the error on the LO term. This should be compared to the precision of the coupling constant in Quantum Electrodynamics (QED), which allows QED series expansions to be kept to 5 loops above leading order before the leading order error drowns out the $\mathrm{N^5LO}$ contributions.

For low-energy regimes such as those encountered in hadrons, Lattice QCD (LQCD) is currently the most popular non-perturbative approach to calculating physical observables. Pioneered in 1974 by Kenneth G. Wilson with his seminal paper "Confinement of Quarks" [2], the method works by reformulating continuum QCD on a four-dimensional hypercubic lattice, allowing the quantum vacuum to be simulated non-perturbatively through the use

of Monte Carlo methods. By measuring vacuum expectation values of relevant operators on the lattice and taking the continuum limit[1], physical quantities such as masses and magnetic moments of hadrons can be extracted to high precision. The lattice method has been hugely successful in verifying [3] and even predicting [4, 5] experimental results, lending good credence to the belief that QCD describes the hadronic world.

These high precision non-perturbative techniques of Lattice QCD offer an enticing way to improve upon the current precision of the strong coupling constant. The goal of this work is to draw lattice data from the literature with the goal of calculating the perturbative expansion parameter $\alpha_s$.

## 1.2 Terminology

In the real world, we know that quarks come in 6 different flavours: up, down, charm, strange, truth, and beauty. In practice, most calculations in QCD employ effective theories to integrate out the spurious degrees of freedom that are introduced when including quark flavours that do not participate in a particular process [6]. This approach works because the process of renormalization introduces an energy scale $\mu$, resulting in the suppression of quark loops involving a quark with mass $m_q > \mu$. Consequently, most variables in QCD are dependent on $n_f$, an effective field theory parameter that counts the number of quarks with mass $m_q < \mu$. In this work, lattice data is drawn from lattice simulations where $n_f = 0$ or $n_f = 2$.

The central focus of this work is the strong coupling constant $\alpha_s$, which depends both on the scale $\mu$ and the number of active fermions $n_f$. By convention, the quoted value is for $n_f = 5$ and the scale is taken to be at the mass of the Z boson. Moreover, the name "strong coupling constant" is decidedly ambiguous – the expansion parameter $\alpha_s$ depends on the chosen scheme used for renormalization. The value of $\alpha_s$ given in eq. (1.1) is in the $\overline{MS}$ scheme, the most popular renormalization scheme used in QCD. This work uses multiple renormalization schemes, and accordingly the expansion parameter in a particular scheme will hereafter be clearly labelled by $\alpha_S$.

## 1.3 Context For This Work

The specific methods used in this work were previously implemented by the QCDSF-UKQCD collaboration [7, 8, 9, 10], however in the intervening time an updated value for the Sommer parameter $r_0$ has been published [11]. It has also come to light that the $n_f = 2$ lattice data contained $r_0/a$ values that were too small [12, 13]. This work closely follows the method of [10], but contributes an exact closed form expression for the integral of the renormalization group equation, modifies an existing method of crossing the strange threshold, and updates the value for $\alpha_{\overline{MS}}$ based on the new values for $r_0$ and $r_0/a$.

It should be noted that the datasets herein, collected from the literature, are from studies using $n_f = 0$ and $n_f = 2$ active fermions, whereas current state-of-the-art studies use

[1] By construction, in the limit that the lattice spacing $a \to 0$, the discretized theory reduces to the continuum theory.

lattice configurations with $n_f = 2 + 1$ [14, 15] and even $n_f = 2 + 1 + 1$ [16, 17]. Due to the complications involved with crossing the strange threshold, these many flavour simulations are better suited to precision measurements of $\alpha_{\overline{MS}}^{(n_f=5)}(m_Z)$. Accordingly, this work is primarily motivated by the updated $r_0$ and $r_0/a$ values, and is not meant to reflect the current capabilities of Lattice QCD.

The structure of this paper is organized as follows. Chapter 2 showcases the mathematics used to extract results from the lattice data. Chapter 3 tabulates the data taken from various sources in the literature and reveals the results that can be drawn from the data. Chapter 4 discusses the overall quality level of this paper, and takes a look at how the results presented here agree with values from the literature. Chapter 5 recapitulates the work, and concludes.

# Chapter 2

# Theory

The goal of this chapter is to elucidate the concepts and methods required to calculate $\alpha_{\overline{MS}}$ from lattice data. Rather than presenting the material in the order in which calculations take place, an attempt has been made to put concepts in an order which should make sense to a reader not familiar with Lattice QCD. To begin, §2.1 outlines the quantum action used to generate the datasets tabulated in Chapter 3, and introduces the Sommer parameter $r_0$. In §2.2, the scale dependence of $\alpha_S$ is determined by integrating the beta function, which introduces the fundamental $\Lambda$ parameter. For renormalization schemes where the four loop beta function coefficient $\beta_3^S$ is not known, a method for estimating its value is described. In §2.3, equations are presented for determining $\alpha_{\overline{MS}}$ when the coupling constant $\alpha_S$ is known in another scheme. Particular attention is paid to the bare lattice scheme and the boosted coupling scheme. §2.4 presents three methods that each allow for the determination of the continuum $\Lambda_{(0)}$ and $\Lambda_{(2)}$ parameters from the bare lattice data. Finally, §2.5 details the intricacies of running $\alpha_{\overline{MS}}$ up to the mass of the Z-boson. By matching the force between static quarks across the strange threshold, it is shown how $\Lambda_{(3)}^{\overline{MS}}$ may be determined using $\Lambda_{(0)}^{\overline{MS}}$ and $\Lambda_{(2)}^{\overline{MS}}$ as input. It is then shown how the charm and beauty thresholds are crossed by writing down a perturbative expression for the discontinuity of $\alpha_{\overline{MS}}$ at the relevant matching scales.

## 2.1 Lattice Details

While no lattice simulations were performed by the author in the completion of this work, it remains necessary to briefly outline some definitions and variables used to generate vacuum configurations and calculate quantities on the lattice.

### 2.1.1 The Lattice Action

All simulations use the standard gauge field action [7]

$$\mathcal{S}_G = \beta \sum_{x \in \Lambda} \frac{1}{3} \mathrm{Tr}\left(U_\Box(x)\right), \tag{2.1}$$

where $\beta \equiv 3/2\pi\alpha_0$, not be confused with the beta function, fixes the coupling constant in the bare lattice scheme (denoted by the '0' subscript). The sum is over the set of

lattice sites, and $U_\Box$ is the plaquette, the sum over all nearest-neighbour Wilson loops originating from lattice site $x$.

When fermions are put on the lattice Wilson fermions are used, which come equipped with the action [18]

$$\mathcal{S}_{\text{Wilson}} = a^4 \sum_{f=1}^{n_f} \sum_{x,y\in\Lambda} \overline{\psi}^{(f)}(x) D^{(f)}(x,y;U) \psi^{(f)}(y), \tag{2.2}$$

where $D^{(f)}(x,y;U)$ is Wilson's lattice Dirac operator. As in the continuum theory, the lattice Dirac operator contains a term proportional to the bare quark mass $am_q$, which is commonly paramaterized by the hopping parameter $\kappa$ and its critical value $\kappa_c$ via the relation

$$am_q = \frac{1}{2}\left(\frac{1}{\kappa} - \frac{1}{\kappa_c}\right). \tag{2.3}$$

The Wilson fermion action suffers from $\mathcal{O}(a)$ discretization errors, which can be removed by using the $\mathcal{O}(a)$ improved Sheikholeslami-Wohlert (clover) action [18, 19, 20]

$$\mathcal{S}_{\text{clover}} = i c_{sw} \frac{a^5}{4} \sum_{x\in\Lambda} \overline{\psi}(x) \sigma_{\mu\nu} F_{\mu\nu}(x) \psi(x). \tag{2.4}$$

The Sheikholeslami-Wohlert coefficient has been determined non-perturbatively, and is best described by the rational equation [19, 21]

$$c_{sw}(\alpha_0) = \frac{1 - 5.705\alpha_0 - 27.63\alpha_0^2 + 23.81\alpha_0^3 + 1122\alpha_0^4}{1 - 9.048\alpha_0}. \tag{2.5}$$

### 2.1.2 The Sommer Parameter $r_0$

One of the most important variables used in this paper is the Sommer parameter $r_0$ [22]. In general, lattice calculations use dimensionless parameters (e.g. masses $am_q$, $am_\pi$, $a\mu$ and lengths $r/a$, $L/a$ ), so a physical quantity is needed to make a connection to the real world. $r_0$ provides one possible method for setting the physical scale of lattice calculations. The definition of $r_0$ is given in terms of the force $f(r)$ between two static quarks, and is expressed as

$$r_0^2 f(r_0) = 1.65. \tag{2.6}$$

A recent determination of $r_0$ [11] gives the value that will be used in this work,

$$\begin{aligned} r_0 &= 0.501(10)(11) \text{ fm} \\ &= 2.538(51)(56) \text{ GeV}^{-1}. \end{aligned} \tag{2.7}$$

One particularly useful quantity related to $r_0$ is the ratio $r_0/a$. It can be calculated on the lattice independent from any knowledge of $r_0$ itself [18], and allows lattice quantities written in terms of an unknown lattice spacing $a$ to be rewritten in term of a known value $r_0$. $r_0/a$ is one of the few variables held in the datasets of this paper, and is central to the determination of $\Lambda_{(n_f)}^{\overline{MS}}$, from which $\alpha_{\overline{MS}}^{(n_f)}$ follows immediately, as is shown in the following section.

## 2.2 Scale Dependence and the Lambda Parameter

In this section the scale dependence of $\alpha_S$ is introduced via the renormalization group equation, and it is shown how the beta function may be integrated analytically, giving rise to the fundamental parameter $\Lambda$. Rational approximants are then introduced as a way to estimate the 4-loop beta function coefficient in renormalization schemes where only three-loop results are known.

### 2.2.1 The Renormalization Group

The process of renormalizing QCD introduces a mass scale $\mu$ and an effective field theory parameter $n_f$ on which the parameters of the theory depend. These parameters are, namely, the strong coupling constant $\alpha_S(\mu; n_f)$ and the masses $m_q^S(\mu; n_f)$ of each of the quarks. Focusing on the scale dependence of $\alpha_S(\mu; n_f)$, the running of the strong coupling constant is governed by the QCD beta function. In an arbitrary scheme $S$, the beta function is defined via the renormalization group equation

$$\frac{d\,\alpha_S^{(n_f)}(\mu)}{d\ln\mu^2} = -(\alpha_S^{(n_f)}(\mu))^2 \sum_{k=0}^{\infty} \beta_k^S(n_f)(\alpha_S^{(n_f)}(\mu))^k \equiv \beta^S(\alpha_S^{(n_f)}(\mu)). \tag{2.8}$$

For the sake of brevity, the functional dependences of $\beta_k^S(n_f)$ and $\alpha_S^{(n_f)}(\mu)$ will hereafter be suppressed. In general, the coefficients $\beta_k$ are dependent on the scheme chosen to renormalize the theory; exceptionally, however, $\beta_0$ and $\beta_1$ are scheme independent. In the $\overline{MS}$ scheme the first four beta function coefficients are known [23, 24], and with the standard normalization of the $SU(3)$ generators, these coefficients are

$$\begin{aligned}
\beta_0 &= \left(\frac{1}{4\pi}\right)\left[\,11 - \frac{2}{3}n_f\,\right] \\
\beta_1 &= \left(\frac{1}{4\pi}\right)^2\left[\,102 - \frac{38}{3}n_f\,\right] \\
\beta_2^{\overline{MS}} &= \left(\frac{1}{4\pi}\right)^3\left[\,\frac{2857}{2} - \frac{5033}{18}n_f + \frac{325}{54}n_f^2\,\right] \\
\beta_3^{\overline{MS}} &= \left(\frac{1}{4\pi}\right)^4\left[\,\frac{149753}{6} + 3564\zeta_3 - \left(\frac{1078361}{162} + \frac{6508}{27}\right)n_f \right. \\
&\qquad \left. - \left(\frac{50065}{162} + \frac{6472}{81}\zeta_3\right)n_f^2 - \frac{1093}{729}n_f^3\,\right],
\end{aligned} \tag{2.9}$$

where, $\zeta_3 \approx 1.20205690$ is Riemann's zeta function evaluated at $z = 3$. Integrating equation 2.8 introduces an arbitrary integration constant that depends mostly on convention [25], but following the convention used by the FLAG Working Group [13], the solution to eq. (2.8) is

$$\frac{\mu}{\Lambda_{n_f}^S} = \exp\left(\frac{1}{2\beta_0\alpha_S}\right)(\beta_0\alpha_S)^{\frac{\beta_1}{2\beta_0^2}} \exp\left[\frac{1}{2}\int_0^{\alpha_S} d\alpha'\left(\frac{1}{\beta(\alpha')} + \frac{1}{\beta_0\alpha'^2} - \frac{\beta_1}{\beta_0^2\alpha'}\right)\right]. \tag{2.10}$$

If written in terms of the roots of the beta function, the integral in eq. (2.10) can be performed analytically to any finite order in perturbation theory. To one loop order, only

$\beta_0$ is non-zero, and eq. (2.10) reduces to

$$\frac{\mu}{\Lambda^S_{(n_f)}} = \exp\left(\frac{1}{2\beta_0\alpha_S}\right), \tag{2.11}$$

Before moving on to the general L-loop case, the integration constant $\Lambda^S_{(n_f)}$ should be given a better introduction. Equation (2.11) shows that in the limit $\mu \to \Lambda^S_{(n_f)}$, the coupling constant $\alpha_S \to \infty$, making any perturbative expansion in $\alpha_S$ divergent. This limit is only strictly obeyed in the 1-loop case, but the qualitative behaviour remains the same for higher loop orders; as $\mu \to \Lambda^S_{n_f}$, $\alpha_S$ becomes large, prohibiting its use as a perturbative expansion parameter. This is why perturbation theory fails to explain hadronic processes – the typical energy scale of hadrons $\mu_{\text{had}} \approx \Lambda^{\overline{MS}}_{(n_f)}$, dooming any chance of writing down a convergent series in $\alpha_{\overline{MS}}$

It should be made clear that $\Lambda^S_{(n_f)}$ is of central importance for determining $\alpha_S$. It is the only parameter that determines how $\alpha_S$ runs with scale $\mu$, and thus can be considered more fundamental than $\alpha_S$ itself. Once $\Lambda^S_{(n_f)}$ is known, $\alpha_S^{(n_f)}(\mu)$ can be easily determined. Consequently, the majority of this work's analysis focuses on determining physical $\Lambda^{\overline{MS}}_{(0)}$ and $\Lambda^{\overline{MS}}_{(2)}$ , and extrapolating those values to $n_f = 5$.

To higher orders, the integration procedure depends on finding the roots of the beta function. Letting $N$ denote the index of the last non-vanishing coefficient $\beta_k$, the Abel-Ruffini theorem implies that this factorization can be done algebraically for $N \leq 4$ (up to 5 loops). For $N \geq 5$, the root-finding must be done numerically. Rewriting the beta function in terms of its non-zero roots $r_k$

$$\beta^S(\alpha_S) = -\beta_N \alpha_S^2 \prod_{k=1}^{N} (\alpha_S - r_k), \tag{2.12}$$

then the partial fraction decomposition for the reciprocal of this rewritten beta function is

$$\frac{1}{-\beta_N \alpha_S^2} \prod_{k=1}^{N} \frac{1}{\alpha_S - r_k} = \frac{A}{\alpha_S} + \frac{B}{\alpha_S^2} + \sum_{k=1}^{N} \frac{P_k^S}{\alpha_S - r_k}, \tag{2.13}$$

with

$$\begin{aligned} A &= \frac{(-1)^{N+1}}{\beta_N} \left[\prod_{k=1}^{N} \frac{1}{r_k}\right] \left[\sum_{k=1}^{N} \frac{1}{r_k}\right] \\ B &= \frac{(-1)^{N+1}}{\beta_N} \prod_{k=1}^{N} \frac{1}{r_k} \\ P_k^S &= -\frac{1}{\beta_N r_k^2} \prod_{\substack{j=1 \\ j\neq k}}^{N} \frac{1}{r_k - r_j}. \end{aligned} \tag{2.14}$$

By multiplying out the product in eq. (2.12) and collecting powers of $\alpha_S$, it can be shown that the expressions for $A$ and $B$ simplify to $A = \beta_1/\beta_0^2$ and $B = -1/\beta_0$. These values

for $A$ and $B$ allow the singular terms of eq. (2.10) to be exactly cancelled, regardless of expansion order. Using these results, eq. (2.10) may be written as

$$\frac{\mu}{\Lambda^S_{(n_f)}} = \exp\left(\frac{1}{2\beta_0\alpha_S}\right)(\beta_0\alpha_S)^{\frac{\beta_1}{2\beta_0^2}} \prod_{k=1}^{N}\left(1-\frac{\alpha_S}{r_k}\right)^{\frac{P_k^S}{2}}. \tag{2.15}$$

This expression holds provided none of the roots $r_k$ are repeated. The nonzero roots of the beta function are, in general, complex, but the imaginary component of eq. (2.15) vanishes exactly, as it must for a purely real integral. One should be aware, however, that computational rounding errors can introduce a small imaginary component when evaluating the expression numerically. Taking the real part of the result solves any problems that may be connected to this issue.

For later convenience, the RHS of eq. (2.15) is defined as the function

$$M^S_{(n_f)}(\alpha_S) = \exp\left(\frac{1}{2\beta_0\alpha_S}\right)(\beta_0\alpha_S)^{\frac{\beta_1}{2\beta_0^2}} \prod_{k=1}^{N}\left(1-\frac{\alpha_S}{r_k}\right)^{\frac{P_k^S}{2}}. \tag{2.16}$$

Unfortunately, $M^S(\alpha_S)$ cannot be inverted analytically to solve for $\alpha_S(\mu)$. Some researchers iteratively invert the expression by writing $\alpha_S(\mu)$ as a series expansion in inverse powers of $\ln(\mu/\Lambda^S_{n_f})$ [1, 25], but for the purposes of this paper a numerical inversion is sufficient.

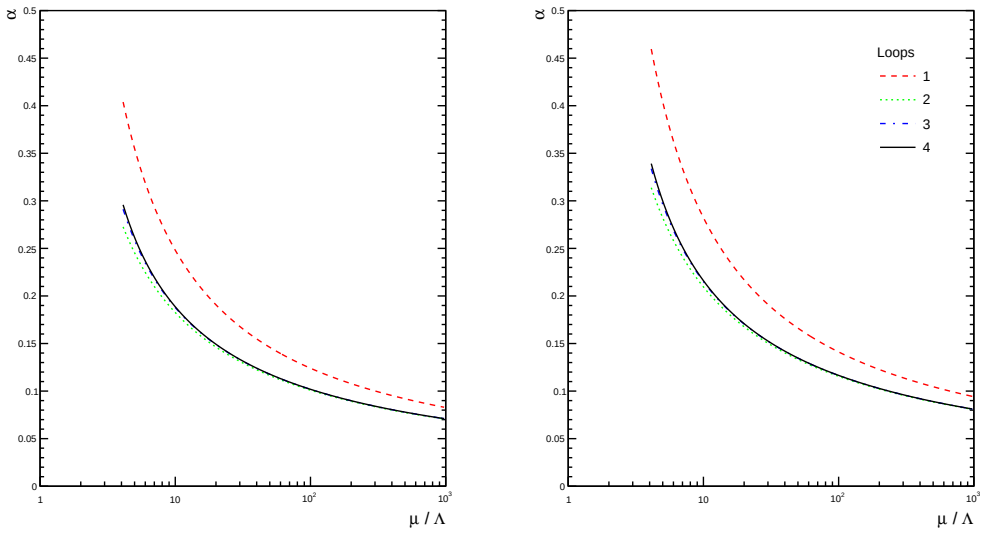


Figure 2.1: $\alpha_{\overline{MS}}$ vs. $\mu/\Lambda^{\overline{MS}}_{(n_f)}$ for $n_f = 0$ (left) and $n_f = 2$ (right), using increasingly higher orders in the perturbative expansion of the beta function.

In §2.3, the series expansion of the natural logarithm of eq. (2.16) is required to derive a useful result. From the asymptotic relation [26]

$$M^S_{(n_f)}(\alpha_S) = \exp\left(\frac{1}{2\beta_0\alpha_S}\right)(\beta_0\alpha_S)^{\frac{\beta_1}{2\beta_0^2}}\left(1-q\alpha_S+\mathcal{O}(\alpha_S^2)\right), \tag{2.17}$$

where

$$q = \frac{\beta_1^2 - \beta_0 \beta_2^S}{2\beta_0^3}, \tag{2.18}$$

it can easily be seen that

$$\sum_{k=1}^{N} \frac{P_k^S}{2} \ln\left(1 - \frac{\alpha_S}{r_k^S}\right) = \ln\left(1 - q\alpha_S + \mathcal{O}(\alpha_S^2)\right). \tag{2.19}$$

By expanding the natural logarithm in its power series and matching powers of $\alpha_S$, the identity

$$\sum_{k=1}^{N} \frac{P_k^S}{2r_k} = q \tag{2.20}$$

is derived. This identity will play a key role in deriving a relation allowing the 3-loop beta function coefficient to be calculated in the lattice and boosted coupling schemes.

### 2.2.2 Padé Approximants

In the overwhelming majority of renormalization schemes, the QCD beta function is not known to four-loop order. Rather than leaving the beta function truncated to 3-loop order, the method of Padé approximants [27] can be used to estimate the 4-loop coefficient $\beta_3$. The goal is to sizably reduce the truncation error while minimizing any errors that might be generated in this estimation procedure.

In general, if a function $f(x)$ is given by the *true* Taylor series,

$$f(x) \approx \sum_{i=0}^{\infty} c_i x^i \tag{2.21}$$

but the coefficients $c_i$ are only known up to some index $N$, then the "best" [28] approximation of the function $f(x)$ is given by the $[L/M]$ Padé approximant

$$f_{[L/M]}(x) \approx \frac{\sum_{i=0}^{L} p_i x^i}{1 + \sum_{j=1}^{M} q_j x^j}, \tag{2.22}$$

where $L + M = N$. The coefficients $p_i$ and $q_j$ are constructed in such a way that when the denominator is expanded out, the resulting coefficients of $x^n$ are pairwise equal to the coeffients $c_n$ for $n \leq N$. The next coefficient of the true Taylor series expansion, $c_{N+1}$, is then estimated by the corresponding coefficient of $x^{N+1}$.

Concretely, the 3-loop beta function is written

$$\beta^S(\alpha_S) = -\beta_0 \alpha_S^2 - \beta_1 \alpha_S^3 - \beta_2^S \alpha_S^4, \tag{2.23}$$

so the *true* beta function is best estimated by the [3/1] Padé approximant

$$\beta^S_{[3/1]}(\alpha_S) = -\frac{\beta_0 \alpha_S^2 + \left(\beta_1 - \frac{\beta_0 \beta_2^2}{\beta_1}\right) \alpha_S^3}{1 - \frac{\beta_2^S}{\beta_1} \alpha_S}. \tag{2.24}$$

Expanding out the denominator of eq. (2.24) reveals that the Padé approximant estimates $\beta_3 \approx \beta_2^2/\beta_1$. To lend confidence to this method, the true and estimated values of $\beta_3^{\overline{MS}}$ are given. For $n_f = 0$, the true value of $\beta_3$ is 1.17, while the estimate is $\beta_2^2/\beta_1 = 0.80$. For $n_f = 2$, the exact value of $\beta_3$ is 0.68, while the Padé method estimates $\beta_2^2/\beta_1 = 0.42$. Clearly the method leaves something to be desired, but at least the values are on the same order of magnitude. This estimation procedure will be used in §2.4, where the beta function of the lattice scheme is known only to 3 loops.

Some experts [10] hold the Padé approximation in high esteem, and in this author's opinion give undue weight to the results produced using this estimation procedure. This paper takes a more conservative approach and will weight all results equally, whether Padé improved or not.

## 2.3 Converting Between Renormalization Schemes

In this work, three renormalization schemes are used: the $\overline{MS}$ scheme, the bare lattice scheme (denoted by the '0' subscript), and the *boosted coupling* scheme (denoted by the '$\Box$' subscript). The bare lattice coupling $\alpha_0$ is put in by hand to the simulation, while the boosted coupling $\alpha_\Box$ is defined as [29]

$$\alpha_\Box \equiv \frac{\alpha_0}{P}, \tag{2.25}$$

where

$$P \equiv \left\langle \frac{\text{Tr } U_\Box}{3} \right\rangle \tag{2.26}$$

is the average plaquette. The purpose of this section is to present the tools necessary to calculate $\alpha_{\overline{MS}}$ given either $\alpha_0$ or $\alpha_\Box$.

### 2.3.1 General Considerations

In general, a coupling constant $\alpha'$ in one renormalization scheme[1] can be written in terms of the coupling constant $\alpha_S$ of another scheme via the perturbative series expansion

$$\alpha'(\mu') = \alpha_S(\mu_S)\left(1 + \sum_{n=1}^{\infty} d_n^S(\mu';\mu_S)\alpha_S^n(\mu_S)\right). \tag{2.27}$$

In some cases, the reciprocal of eq. (2.27) is also needed. Expanded out in a truncated series, this inverse relation reads

$$\frac{1}{\alpha'} = \frac{1}{\alpha_S} - d_1^S - \alpha_S\left[d_2^S - (d_1^S)^2\right] - \alpha_S^2\left[d_3^S - 2d_1^S d_2^S + (d_1^S)^3\right] + \mathcal{O}(\alpha_S^3). \tag{2.28}$$

[1]Throughout §2.3 the number of active fermions will be assumed to be the same when converting between schemes.

Not much can be done with these series expansions alone. The path to deriving useful relations begins by taking the natural logarithm of $M'(\alpha')$ (eq. (2.16)) and expanding the expression in a power series in $\alpha_S$ using equations (2.27) and (2.28):

$$\begin{aligned}\ln M'(\alpha') &= \frac{1}{2\beta_0\alpha'} + \frac{\beta_1}{2\beta_0^2}\ln(\beta_0\alpha') + \sum_{k=1}^{N}\frac{P'_k}{2}\ln\left(1-\frac{\alpha'}{r'_k}\right) \\ &= \frac{1}{2\beta_0}\left\{\frac{1}{\alpha_S} - d_1^S - \alpha_S\left[d_2^S - (d_1^S)^2\right] + \mathcal{O}(\alpha_S^2)\right\} \\ &\quad + \frac{\beta_1}{2\beta_0^2}\ln(\beta_0\alpha_S) + \frac{\beta_1}{2\beta_0^2}\ln\left(1 + d_1^S\alpha_S + \mathcal{O}(\alpha_S^2)\right) \\ &\quad - \sum_{k=1}^{N}\frac{P'_k}{2}\sum_{j=1}^{\infty}\frac{1}{j}\left(\frac{\alpha'}{r_k^S}\right)^j\left(1 + d_1^S\alpha_S + \mathcal{O}(\alpha_S^2)\right)^j.\end{aligned} \tag{2.29}$$

In this form the hints of $\ln M^S(\alpha_S)$ can be discerned. Carefully extracting the relevant terms gives

$$\begin{aligned}\ln M'(\alpha') &= \ln M^S(\alpha_S) - \frac{1}{2\beta_0}\left\{d_1^S + \alpha_S\left[d_2^S - (d_1^S)^2\right] + \mathcal{O}(\alpha_S^2)\right\} \\ &\quad + \frac{\beta_1}{2\beta_0^2}\ln\left(1 + d_1^S\alpha_S + \mathcal{O}(\alpha_S^2)\right) \\ &\quad - \sum_{k=1}^{N}\frac{P'_k}{2}\sum_{j=1}^{\infty}\frac{1}{j}\left(\frac{\alpha'}{r'_k}\right)^j\left(1 + d_1^S\alpha_S + \mathcal{O}(\alpha_S^2)\right)^j \\ &\quad + \sum_{k=1}^{N}\frac{P_k^S}{2}\sum_{j=1}^{\infty}\frac{1}{j}\left(\frac{\alpha'}{r_k^S}\right)^j\left(1 + d_1^S\alpha_S + \mathcal{O}(\alpha_S^2)\right)^j.\end{aligned} \tag{2.30}$$

Using the identity in eq. (2.20), this equation reduces to

$$\begin{aligned}0 &= \ln M^S(\alpha_S) - \ln M'(\alpha') - \frac{d_1^S}{2\beta_0} \\ &\quad + \alpha_S\left\{\left[d_2^S - (d_1^S)^2\right] - \frac{\beta_1}{2\beta_0^2} - q' + q^S\right\} + \mathcal{O}(\alpha_S^2).\end{aligned} \tag{2.31}$$

For this equation to be true for each value of $\alpha_S$, the coefficients of each power of $\alpha_S$ must vanish. For the zeroth power, this implies

$$d_1^S = 2\beta_0\ln\frac{M^S(\alpha_S)}{M'(\alpha')}, \tag{2.32}$$

and recalling that $M^S(\alpha_S) = \mu_S/\Lambda^S$, an extremely useful equation is found:

$$d_1^S = 2\beta_0\ln\frac{\Lambda'}{\Lambda^S} - 2\beta_0\ln\frac{\mu'}{\mu_S}. \tag{2.33}$$

The first term on the RHS is important enough to be assigned its own variable,

$$t_1^S \equiv 2\beta_0\ln\frac{\Lambda'}{\Lambda^S}. \tag{2.34}$$

$t_1^S$ can be determined by a 1-loop calculation [30], and thus the conversion between $\Lambda$ parameters is fully determined by NLO perturbation theory.

After a few lines of algebra, the vanishing of the $\mathcal{O}(\alpha_S)$ term reveals

$$d_2^S = \frac{\beta_1 t_1^S + \beta_2' - \beta_2^S}{\beta_0} - 2\beta_1 \ln \frac{\mu'}{\mu_S} + (d_1^S)^2. \tag{2.35}$$

The first term on the RHS is again important enough to assign its own variable, $t_2^S$. The determination of $t_2^S$ requires a 2-loop calculation, and once it is found, the 3-loop beta function coefficient $\beta_2^S$ can be acquired via

$$\beta_2^S = \beta_2' + \beta_1 t_1^S - \beta_0 t_2^S. \tag{2.36}$$

A similar relation can be derived for $\beta_3^S$ in terms of a new coefficient $t_3^S$ [10], but for the purposes of this work it is not required. As an aside, however, if $t_3^S$ were known, the 4-loop beta function coefficient $\beta_3^S$ could be computed, taking away the need for the Padé approximation method of §2.2.2. This concludes the general discussion of converting between renormalization schemes, the ideas of which will be used in the following section to convert $\alpha_0$ to $\alpha_{\overline{MS}}$.

### 2.3.2 From the Bare Lattice Scheme to the $\overline{MS}$ Scheme

The conversion variables $t_1^0$ and $t_2^0$ of the bare lattice scheme are functionally dependent on two lattice parameters: the Sheikholeslami-Wohlert coefficient $c_{sw}$ of eq. (2.4), and the bare quark mass $am_q$. Their values are [7]

$$\begin{aligned} t_1^0 &= (4\pi)\left\{0.4682013 - n_f[0.0066960 - 0.0050467c_{sw} + 0.0298435c_{sw}^2 \right. \\ &\qquad \left. -am_q(0.0272837 - 0.0223503c_{sw} + 0.0070667c_{sw}^2) + \mathcal{O}((am_q)^2)]\right\} \\ t_2^0 &= (4\pi)^2\left\{0.556675 - n_f[0.002600 + 0.000155c_{sw} - 0.012834c_{sw}^2 \right. \\ &\qquad \left. -0.000474c_{sw}^3 - 0.000103c_{sw}^4 + \mathcal{O}(am_q)]\right\}. \end{aligned} \tag{2.37}$$

In this paper, these equations are never used as written here. Before converting to the $\overline{MS}$ scheme, the $\mathcal{O}((am_q)^n)$ correction terms are made to vanish for $n \geq 1$ by first extrapolating to the chiral limit $am_q \to 0$.

In any lattice scheme the inverse lattice spacing $1/a$ takes the place of the continuum scale $\mu$. The conversion coefficients $d_1^0$ and $d_2^0$ are then

$$\begin{aligned} d_1^0 &= t_1^0 - 2\beta_0 \ln(a\mu) \\ d_2^0 &= t_2^0 - 2\beta_1 \ln(a\mu) + (d_1^0)^2. \end{aligned} \tag{2.38}$$

### 2.3.3 From the Boosted Lattice Scheme to the $\overline{MS}$ Scheme

Even though the conversion between the bare coupling scheme and the $\overline{MS}$ scheme is known to two loop order, the series is poorly convergent [10, 31]. To *boost* the convergence between schemes, the *boosted* coupling $\alpha_\square$, defined in eq. (2.25), is used. To further

improve the convergence of the series, the tadpole improved Sheikholeslami-Wohlert coefficient $c_{sw}^{\square}$ is used [10], defined as

$$c_{sw}^{\square} \equiv c_{sw} P^{3/4}. \tag{2.39}$$

Then the conversion variables $t_1^{\square}$ and $t_2^{\square}$ in the boosted coupling scheme are written as

$$\begin{aligned} t_1^{\square} &= (4\pi)\left\{0.1348680 - n_f[0.0066960 - 0.0050467 c_{sw}^{\square} + 0.0298435 (c_{sw}^{\square})^2 \right. \\ &\qquad \left. - am_q(0.0272837 - 0.0223503 c_{sw}^{\square} + 0.0070667 (c_{sw}^{\square})^2) + \mathcal{O}((am_q)^2)]\right\} \\ t_2^{\square} &= (4\pi)^2\left\{0.556675 - n_f[0.002600 + 0.000155 c_{sw} - 0.012834 (c_{sw}^{\square})^2 \right. \\ &\qquad \left. - 0.000474 (c_{sw}^{\square})^3 - 0.000103 (c_{sw}^{\square})^4 + \mathcal{O}(am_q)]\right\}. \end{aligned} \tag{2.40}$$

As with the bare coupling conversion, these equations are never used in the form written here – an extrapolation to the chiral limit is first done to remove the $\mathcal{O}((am_q)^n)$ terms for $n \geq 1$. The form of the conversion coefficients $d_1^{\square}$ and $d_2^{\square}$ is then the same as in eq. (2.38).

## 2.4 Three Methods

This section introduces three methods of determining $\Lambda_{(0)}^{\overline{MS}}$ and $\Lambda_{(2)}^{\overline{MS}}$ from lattice data. The methods are the same as those used in [10]. When working in the quenched approximation ($n_f = 0$), the only data required are the values of the coupling $\beta$, the average plaquette $P$, and the dimensionless inverse lattice spacing $r_0/a$. In the case that there are fermions on the lattice, the hopping parameter $\kappa$ and its critical value $\kappa_c$ are also needed as input. Before any of the following methods are used, the $n_f = 2$ data is extrapolated to the chiral limit $am_q \to 0$ (or equivalently $\kappa \to \kappa_c$) in order to reduce quark mass effects.

The central equation of the three methods is

$$r_0 \Lambda_{(n_f)}^{\overline{MS}} = r_0 \mu \frac{1}{M_{(n_f)}^{\overline{MS}}(\alpha_{\overline{MS}}(\mu))}, \tag{2.41}$$

which follows from the equality of eqs. (2.15) and (2.16). The factor of $r_0$ was multiplied on each side in order to make use of $r_0/a$ values calculated on the lattice. Once the dimensionless variable $r_0 \Lambda_{(n_f)}^{\overline{MS}}$ is calculated, the dimensionful parameter $\Lambda_{(n_f)}^{\overline{MS}}$ can be calculated using the known value of $r_0$ (see eq. (2.7)).

### 2.4.1 Method I

This method is the most direct of the three. The bare lattice coupling is determined from $\beta$ via eq. (2.8), and is then converted to $\alpha_{\overline{MS}}$ via eq. (2.27), where $d_1$ and $d_2$ are found using eq. 2.38. In order to reduce the error that stems from the conversion from the bare lattice scheme to the $\overline{MS}$ scheme, the scale $\mu$ at which the scheme conversion is performed is chosen to set $d_1 = 0$. The desired consequence of this choice is that the correction to the scheme conversion begins at $\mathcal{O}(\alpha_0^3)$. To achieve this, the scale is set to

$$\mu_{\text{I}}^0 = \frac{1}{a} \exp\left(\frac{t_1^0}{2\beta_0}\right), \tag{2.42}$$

which results in the second conversion coefficient $d_2^0$ reducing to

$$d_2^0 = t_2^0 - \frac{\beta_1}{\beta_0} t_1^0. \tag{2.43}$$

Inserting the scale $\mu_{\text{I}}$ into the central equation (2.41), this method of calculating $r_0\Lambda_{(n_f)}^{\overline{MS}}$ can be summarized by the equation

$$r_0\Lambda_{(n_f)}^{\overline{MS}} = \left(\frac{r_0}{a}\right) \exp\left(\frac{t_1^0}{2\beta_0}\right) \frac{1}{M_{(n_f)}^{\overline{MS}}(\alpha_{\overline{MS}}\,(\mu_{\text{I}}^0))}. \tag{2.44}$$

This method concludes with an extrapolation to the continuum limit $a \to 0$.

Naïvely one would expect this method to work rather well. However, examining the results that this produces in Figure 3.1a, one can see that there is a high degree of nonlinearity in the behaviour of $r_0\Lambda_{(0)}^{\overline{MS}}$ as $a \to 0$, even at small lattice spacings. This is the primary motivation for using the boosted coupling, since a reliable extrapolation to the continuum limit is of the utmost importance.

This method is the same for the boosted coupling approach, except once the bare coupling is found eq. 2.25 is used to calculate $\alpha_{\square}$. The conversion coefficients $d_1^{\square}$ and $d_2^{\square}$ are calculated using the corresponding $t_1^{\square}$ and $t_2^{\square}$ variables, and the scale is set with the same requirement that $d_1^{\square}$ must vanish. After using

$$r_0\Lambda_{(n_f)}^{\overline{MS}} = \left(\frac{r_0}{a}\right) \exp\left(\frac{t_1^{\square}}{2\beta_0}\right) \frac{1}{M_{(n_f)}^{\overline{MS}}(\alpha_{\overline{MS}}\,(\mu_{\text{I}}^{\square}))}, \tag{2.45}$$

for various lattice spacings, the continuum limit is taken. Figure 3.1b shows how much better this approach works with the boosted coupling than with the bare lattice coupling. Consequently, the remaining two methods will only make use of the boosted coupling, and the final value of $r_0\Lambda_{(n_f)}^{\overline{MS}}$ will be determined by taking into consideration only those values found using the boosted coupling approach.

With respect to the chosen scale $\mu_{\text{I}}^{\square}$, the stability of the extrapolated value for $r_0\Lambda_{(n_f)}^{\overline{MS}}$ is important. If $r_0\Lambda_{(n_f)}^{\overline{MS}}$ were to vary too much with small variations in the scale, the reliability of the method could be called into question. As a simple stability analysis, the continuum limit value for $r_0\Lambda_{(0)}^{\overline{MS}}$ is plotted in Figure 2.2 as a function of $\mu/\mu_{\text{I}}^{\square}$. It can be seen that the curve is flattest near the scale $\mu = \mu_{\text{I}}^{\square}$, showing that $\mu_{\text{I}}^{\square}$ is, after all, a good choice for the scale. For details on the equations used to find $r_0\Lambda_{(n_f)}^{\overline{MS}}(\mu/\mu_{\text{I}})$, see Appendix A.

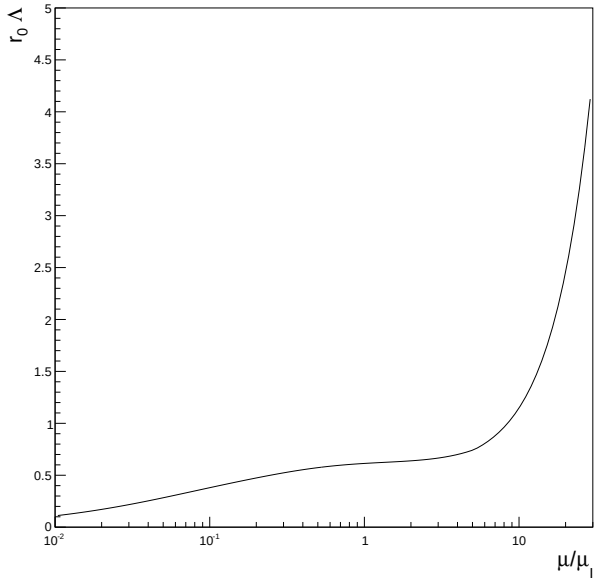


Figure 2.2: Stability analysis for the choice of scale in Method I for $n_f = 0$ with the boosted coupling scheme.

### 2.4.2 Method II

The motivation for this method is to eliminate *all* the correction coefficients $d_n^{\square}$ in eq. (2.27) for $n \geq 1$, effectively setting

$$\alpha_{\overline{MS}}\left(\mu_{\text{II}}\right) = \alpha_{\square}(a). \tag{2.46}$$

For this to occur, the scale must be set to

$$\mu_{\text{II}}^{\square} = \frac{1}{a}\exp\left(\frac{t_1^{\square}}{2\beta_0}\right)\frac{M^{\overline{MS}}\left(\alpha_{\square}(a)\right)}{M^{\square}(\alpha_{\square}(a))}. \tag{2.47}$$

To calculate the quantity $M^{\square}(\alpha_{\square}(a))$ to 3-loop order, the beta function coefficient $\beta_2^{\square}$ must first be determined via eq. (2.36). Thereafter, this method gives

$$r_0\Lambda_{(n_f)}^{\overline{MS}} = \left(\frac{r_0}{a}\right)\exp\left(\frac{t_1^{\square}}{2\beta_0}\right)\frac{M^{\overline{MS}}\left(\alpha_{\square}(a)\right)}{M^{\square}(\alpha_{\square}(a))M^{\overline{MS}}\left(\alpha_{\overline{MS}}\left(\mu_{\text{II}}\right)\right)}, \tag{2.48}$$

where $\alpha_{\square}(a)$ must first be calculated using eq. (2.25). Of course, the factor $M^{\overline{MS}}\left(\alpha_{\square}(a)\right)$ in the denominator cancels the $M^{\overline{MS}}\left(\alpha_{\overline{MS}}\left(a\right)\right)$ factor in the numerator, but the chosen form is particularly well suited for conveying the details of the calculation, and is needed for the stability analysis of the resulting $r_0\Lambda_{(0)}^{\overline{MS}}$ shown in Figure 2.3.

Using the Padé approximant method of §2.2.2, the beta function coefficient $\beta_3^{\square}$ can be estimated, allowing the function $M^{\square}(\alpha_{\square}(a))$ to be calculated to 4-loop order. When this estimation procedure is used, the method is labelled as Method IIP.

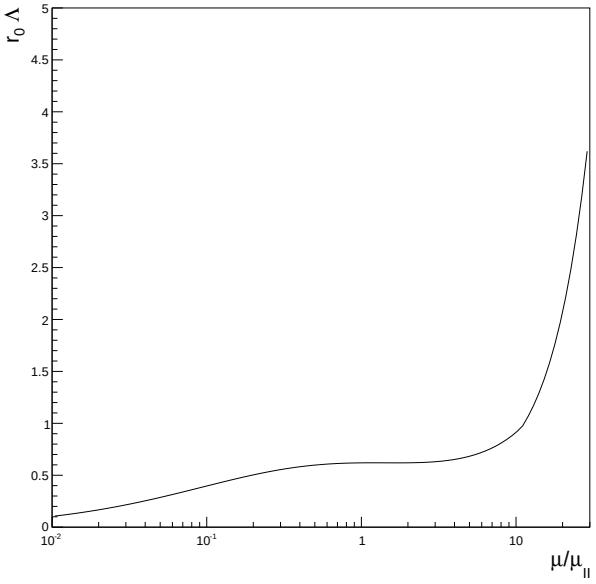


Figure 2.3: Stability analysis for the choice of scale in Method II for $n_f = 0$.

### 2.4.3 Method III

The philosophy of this method is to choose the scale in the same manner as in Method II, but to construct the boosted coefficients $b_i^{\Box}$, $d_j^{\Box}$, and $t_k^{\Box}$ in such a way that they are independent of the coupling $\alpha_{\Box}$. These variables only depend on the coupling through the $c_{sw}^{\Box}$ coefficient, so the strategy is to fix $c_{sw}^{\Box}$ to a constant value while maintaining both its perturbative consistency and its improvement properties. This is done using the perturbative expansion

$$c_{sw}^{\Box} = 1 + c_0^{\Box}\alpha_{\Box} + \mathcal{O}(\alpha_{\Box}^2), \tag{2.49}$$

where $c_0^{\Box} = 0.1998$ [10]. To begin, eq. (2.28) is written in terms of $t_1^{\Box}$ and $t_2^{\Box}$ via eq. (2.38), simplified by setting $a = 1/\mu$, then is differentiated by $\partial/\partial \ln \mu^2$, leaving

$$\beta^{\overline{MS}}(\alpha_{\overline{MS}})\frac{1}{\alpha_{\overline{MS}}^2} = \beta^{\Box}(\alpha_{\Box})\left[\frac{1}{\alpha_{\Box}^2} + \frac{\partial t_1^{\Box}}{\partial c_{sw}^{\Box}}\frac{\partial c_{sw}^{\Box}}{\partial \alpha_{\Box}} + t_2^{\Box} + \mathcal{O}(\alpha_{\Box})\right], \tag{2.50}$$

where the definition of the beta function, eq. (2.8), was used. Expanded out in powers of $\alpha_{\Box}$, it is found that

$$\beta_2^{\Box} = \beta_2^{\overline{MS}} + \beta_1 t_1^{\Box}|_{c_{sw}^{\Box}=1} - \beta_0 t_2^{\Box}|_{c_{sw}^{\Box}=1} - \beta_0 c_0^{\Box}\frac{\partial t_1^{\Box}}{\partial c_{sw}^{\Box}}|_{c_{sw}^{\Box}=1}. \tag{2.51}$$

For this method, this is the equation used to calculate $\beta_2^{\Box}$, rather than eq. (2.36). The scale $\mu_{\text{III}}$ is chosen in the same way as in Method II, but with $t_1^{\Box}$ evaluated at $c_{sw}^{\Box} = 1$, leaving the following equation for calculating $r_0\Lambda_{(n_f)}^{\overline{MS}}$

$$r_0\Lambda_{(n_f)}^{\overline{MS}} = \left(\frac{r_0}{a}\right)\exp\left(\frac{t_1^{\Box}|_{c_{sw}^{\Box}=1}}{2\beta_0}\right)\frac{1}{M^{\Box}(\alpha_{\Box}(a))}, \tag{2.52}$$

where again, $\alpha_{\square}(a)$ must be calculated using eq. (2.25). As with Method II, there is an opportunity to use Padé approximants to estimate the beta function coefficient $\beta_3^{\square}$. When this estimation procedure is used, the method is labelled as Method IIIP.

## 2.5 Crossing the Quark Thresholds

Since the data used in this paper is drawn only from $n_f = 0$ and $n_f = 2$ lattice simulations, the three methods provided in the previous section can only be used to calculate $\Lambda_{(0)}^{\overline{MS}}$ and $\Lambda_{(2)}^{\overline{MS}}$, though $\Lambda_{(5)}^{\overline{MS}}$ is needed to finally determine $\alpha_{\overline{MS}}^{(n_f=5)}(m_Z)$. The scale at which the $n_f = 2$ effective theory no longer applies is at the mass of the strange quark; at scales above this threshold, the $n_f = 3$ effective theory takes over. At this scale $\alpha_{\overline{MS}}$ is large, precluding the use of a perturbative matching calculation between $\alpha_{\overline{MS}}^{(3)}$ and $\alpha_{\overline{MS}}^{(2)}$. Instead, a matching procedure involving the $\Lambda_{(n_f)}^{\overline{MS}}$ parameters is used. In contrast, the direct matching of $\alpha_{\overline{MS}}^{(n_f+1)}$ to $\alpha_{\overline{MS}}^{(n_f)}$ at the charm and beauty thresholds is done perturbatively, since at these scales $\alpha_{\overline{MS}}$ is small enough for the effective use of perturbative methods.

### 2.5.1 Crossing the Strange Threshold

Two quarks held at a distance $r$ from one another experience a force analogous to the Coulomb force experienced by two static electric charges. The static quark potential is known to 3-loop order [32] but only 2-loop results will be used here, since the 3-loop correction is complicated by terms of the form $\alpha_{\overline{MS}}^4 \ln \alpha_{\overline{MS}}$. To 2-loop order, the static quark potential is [33]

$$\begin{aligned} V(r;\alpha_{\overline{MS}}^{(n_f)},\mu) = -\frac{4}{3}\frac{\alpha_{\overline{MS}}^{(n_f)}}{r}\Bigg\{1 + \alpha_{\overline{MS}}^{(n_f)}\left[2\beta_0 \ln(\mu r') + a_1\right] \\ + (\alpha_{\overline{MS}}^{(n_f)})^2\Bigg[\beta_0^2\left(4\ln^2(\mu r') + \frac{\pi^2}{3}\right) \\ +2(\beta_1 + 2\beta_0 a_1)\ln(\mu r') + a_2\Bigg] + \mathcal{O}(\alpha_{\overline{MS}}^3)\Bigg\}, \end{aligned} \tag{2.53}$$

where $r' \equiv re^{\gamma}$ and the two constant $a_1$ and $a_2$ are [34, 35]

$$\begin{aligned} a_1 &= \frac{1}{4\pi}\left[\frac{31}{3} - \frac{10}{9}n_f\right] \\ a_2 &= \frac{1}{(4\pi)^2}\left[\left(\frac{4343}{18} + 36\pi^2 - \frac{9\pi^4}{4} + 66\zeta_3\right) - \left(\frac{1229}{27} + \frac{52}{3}\zeta_3\right)n_f + \frac{100}{81}n_f^2\right]. \end{aligned} \tag{2.54}$$

The force experienced by a second quark at a distance $r$ from the first is calculated from[2] $f(r) = dV/dr$, leading to the expression

[2]Note the opposite sign convention.

$$r^2 f(r) = \frac{4}{3}\alpha_{\overline{MS}} \Bigg\{ 1 + \alpha_{\overline{MS}} \left[ 2\beta_0 \ln(\mu r') + a_1 - 2\beta_0 \right] + \alpha_{\overline{MS}}^2 \Bigg[ \beta_0^2 \left( 4\ln^2(\mu r') - 8\ln(\mu r') + \frac{\pi^2}{3} \right) + 2(\beta_1 + 2\beta_0 a_1)(\ln(\mu r') - 1) + a_2 \Bigg] + \mathcal{O}(\alpha_{\overline{MS}}^3) \Bigg\}. \tag{2.55}$$

Defining a force-scale coupling $\alpha_{q\bar{q}}$ by [36]

$$r^2 f(r) = \frac{4}{3}\alpha_{q\bar{q}}(r), \tag{2.56}$$

the expansion coefficients $d_1^{q\bar{q}}$ and $d_2^{q\bar{q}}$ for the conversion from the force-scale coupling scheme to the $\overline{MS}$ can be shown to be

$$\begin{aligned} d_1^{q\bar{q}} &= 2\beta_0 - a_1 - 2\beta_0 \ln(\mu r') \\ d_2^{q\bar{q}} &= (d_1^{q\bar{q}})^2 - 2\beta_1 \ln(\mu r') + \beta_0^2 \left( 4 - \frac{\pi^2}{3} \right) + 2\beta_1(1-\gamma) + a_1^2 - a_2, \end{aligned} \tag{2.57}$$

which gives the conversion variables $t_1^{q\bar{q}}$ and $t_2^{q\bar{q}}$ as

$$\begin{aligned} t_1^{q\bar{q}} &= 2\beta_0(1-\gamma) - a_1 \\ t_2^{q\bar{q}} &= \beta_0^2 \left( 4 - \frac{\pi^2}{3} \right) + 2\beta_1(1-\gamma) + a_1^2 - a_2. \end{aligned} \tag{2.58}$$

Assuming now that the force $f(r^*)$ between static quarks is $n_f$-independent at some particular distance $r^*$, then from eq. (2.56) so too is $\alpha_{q\bar{q}}(r^*)$. From eqs. (2.15) and (2.16), the relation

$$r^* \Lambda_{(n_f)}^{q\bar{q}} = \frac{1}{M_{(n_f)}^{q\bar{q}}(\alpha_{q\bar{q}})} \tag{2.59}$$

can be used to calculate ratios of $\Lambda^{q\bar{q}}$ that are independent of the $r^*$. Equation (2.34) then converts these ratios of $\Lambda^{q\bar{q}}$ into ratios of $\Lambda^{\overline{MS}}$. Concretely, the ratios

$$\frac{\Lambda_{(2)}^{\overline{MS}}}{\Lambda_{(0)}^{\overline{MS}}} = \frac{\exp\left( \frac{t_{1(2)}^{q\bar{q}}}{2\beta_0^{(2)}} \right) M_{(0)}^{q\bar{q}}(\alpha_{q\bar{q}})}{\exp\left( \frac{t_{1(0)}^{q\bar{q}}}{2\beta_0^{(0)}} \right) M_{(2)}^{q\bar{q}}(\alpha_{q\bar{q}})} \tag{2.60}$$

and

$$\frac{\Lambda_{(3)}^{\overline{MS}}}{\Lambda_{(2)}^{\overline{MS}}} = \frac{\exp\left( \frac{t_{1(3)}^{q\bar{q}}}{2\beta_0^{(3)}} \right) M_{(2)}^{q\bar{q}}(\alpha_{q\bar{q}})}{\exp\left( \frac{t_{1(2)}^{q\bar{q}}}{2\beta_0^{(2)}} \right) M_{(3)}^{q\bar{q}}(\alpha_{q\bar{q}})} \tag{2.61}$$

can be determined as functions of $\alpha_{q\bar{q}}$. By choosing an arbitrary value of $\Lambda_{(2)}^{\overline{MS}} / \Lambda_{(0)}^{\overline{MS}}$, eq. (2.60) can be numerically inverted to give the corresponding value of $\alpha_{q\bar{q}}$. Inputting this

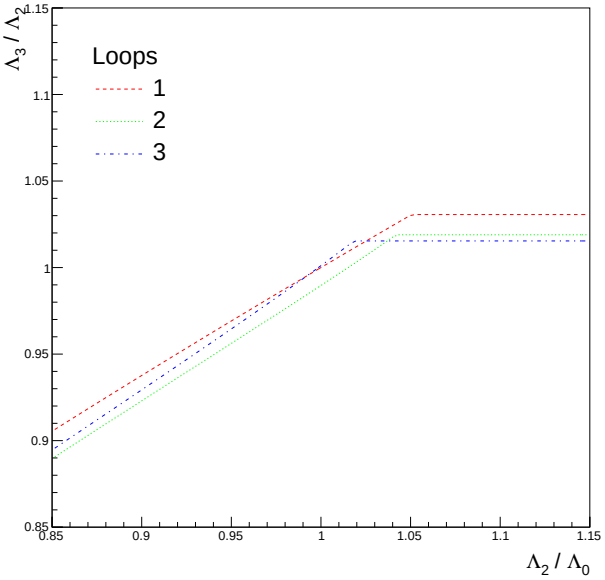


Figure 2.4: $\Lambda_{(3)}^{\overline{MS}} / \Lambda_{(2)}^{\overline{MS}}$ versus $\Lambda_{(2)}^{\overline{MS}} / \Lambda_{(0)}^{\overline{MS}}$.

output into eq. (2.61) thus gives $\Lambda_{(3)}^{\overline{MS}} / \Lambda_{(2)}^{\overline{MS}}$ as a function of $\Lambda_{(2)}^{\overline{MS}} / \Lambda_{(0)}^{\overline{MS}}$. This is shown in Figure 2.4.

Looking at Figure 2.4, something is quite clearly going wrong at $\Lambda_{(2)}^{\overline{MS}} / \Lambda_{(0)}^{\overline{MS}} \sim 1.05$: the smooth curves abruptly become perfectly horizontal. What this represents is the fact that as $\alpha_{q\bar{q}} \to \infty$, $\Lambda_{(2)}^{\overline{MS}} / \Lambda_{(0)}^{\overline{MS}}$ reaches its asymptotic value of $\sim 1.05$. When the numerical inversion algorithm can't find a value for $\alpha_{q\bar{q}}$ that corresponds to a large ($> 1.05$) value of $\Lambda_{(2)}^{\overline{MS}} / \Lambda_{(0)}^{\overline{MS}}$, it outputs the highest value of $\alpha_{q\bar{q}}$ that it is allowed to give. This highest value is then used as input to calculate $\Lambda_{(3)}^{\overline{MS}} / \Lambda_{(2)}^{\overline{MS}}$, producing the horizontal line lying at a y-value equal to the asymptotic value of $\Lambda_{(3)}^{\overline{MS}} / \Lambda_{(2)}^{\overline{MS}}$. This would be fine so long as $\Lambda_{(2)}^{\overline{MS}} / \Lambda_{(0)}^{\overline{MS}} \lesssim 1.05$, as was found in [10], where this matching procedure was used with great success. Unfortunately, the results in Chapter 3 show $\Lambda_{(2)}^{\overline{MS}} / \Lambda_{(0)}^{\overline{MS}} > 1.05$. This is clearly a problem.

To save this method, recall that in the region $\Lambda_{(2)}^{\overline{MS}} / \Lambda_{(0)}^{\overline{MS}} \sim 1.05$, the expansion parameter $\alpha_{q\bar{q}}$ is large. This means that the abrupt cutoff to a horizontal line in Figure 2.4 is just a symptom of perturbation theory breaking down. Consequently, any attempt to predictively use $\alpha_{q\bar{q}}$ in this region should be discouraged. Before this non-perturbative region is reached, however, it is observed that the curves are well-behaved and slowly varying. With no reference to $\alpha_{q\bar{q}}$ anywhere in Figure 2.4, there is no reason to expect this behaviour to change in the region $\Lambda_{(2)}^{\overline{MS}} / \Lambda_{(0)}^{\overline{MS}} > 1.05$. This allows a Taylor series to be constructed, fitting the curves in the the perturbative region and extrapolating to the non-perturbative region.

Believing that the region $\alpha_{q\bar{q}} < 0.5$ should give reliable perturbative results, 20 values of $\Lambda_{(2)}^{\overline{MS}} / \Lambda_{(0)}^{\overline{MS}}$ and $\Lambda_{(3)}^{\overline{MS}} / \Lambda_{(2)}^{\overline{MS}}$ are directly calculated with eqs. (2.60) and (2.61) for $0.025 \leq \alpha_{q\bar{q}} \leq 0.475$. These pairs are fitted with a quartic polynomial in $\Lambda_{(2)}^{\overline{MS}} / \Lambda_{(0)}^{\overline{MS}}$, and expanded about $\Lambda_{(2)}^{\overline{MS}} / \Lambda_{(0)}^{\overline{MS}} = 1.1$, where the expansion point was chosen from the results of Chapter 3. The extrapolated curves are shown in Figure 2.5.

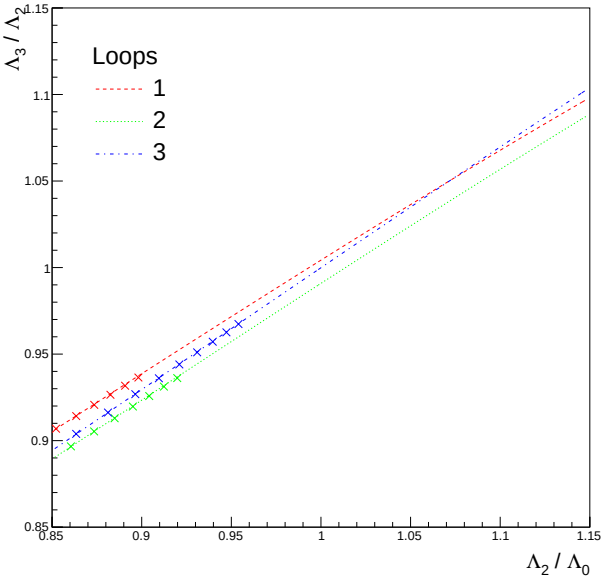


Figure 2.5: Fitted and extrapolated $\Lambda_{(3)}^{\overline{MS}}/\Lambda_{(2)}^{\overline{MS}}$ versus $\Lambda_{(2)}^{\overline{MS}}/\Lambda_{(0)}^{\overline{MS}}$ curves using a quartic series expansion about $\Lambda_{(2)}^{\overline{MS}}/\Lambda_{(0)}^{\overline{MS}} = 1.1$. The X markers denote the points which are used to fit the curves.

### 2.5.2 Crossing the Charm and Beauty Thresholds

At high enough energy scales, matching across quark thresholds can be done perturbatively. The matching condition reads [37]

$$\alpha_{\overline{MS}}^{(n_f+1)}(m_q^{\overline{MS}}) = \frac{1}{\zeta_g^2}\alpha_{\overline{MS}}^{(n_f)}(m_q^{\overline{MS}}), \tag{2.62}$$

where $m_q^{\overline{MS}}$ is the mass of the heavy quark evaluated at the scale $\mu = m_s^{\overline{MS}}$. The prefactor is [38]

$$\frac{1}{\zeta_g^2} = 1 - \frac{11}{72}\left(\frac{\alpha_{\overline{MS}}^{(n_f)}(m_q^{\overline{MS}})}{\pi}\right)^2 + \left(\frac{\alpha_{\overline{MS}}^{(n_f)}(m_q^{\overline{MS}})}{\pi}\right)^2\left(-\frac{564731}{124416} + \frac{82043}{27648}\zeta_3 + \frac{2633}{31104}n_f\right). \tag{2.63}$$

Thus once the parameter $\Lambda_{(3)}^{\overline{MS}}$ is determined the process is as follows: $\alpha_{\overline{MS}}^{(n_f=3)}(m_c^{\overline{MS}})$ is determined by inverting eq. (2.15), then $\alpha_{\overline{MS}}^{(n_f=4)}(m_c^{\overline{MS}})$ is determined by matching across the charm threshold with eq. (2.62), and $\Lambda_{(4)}^{\overline{MS}}$ is then found by once again using eq. (2.15). This process is repeated to cross the bottom threshold, leading to a determination of $\Lambda_{(4)}^{\overline{MS}}$. Finally, eq. (2.15) is inverted again to find $\alpha_{\overline{MS}}^{(n_f=5)}(m_Z)$.

The Z boson mass and $\overline{MS}$ quark masses are drawn from the PDG review [1]. The values used are

$$m_Z = 91.1876(21) \quad ; \quad m_c^{\overline{MS}}(m_c^{\overline{MS}}) = 1.275(25) \quad ; \quad m_b^{\overline{MS}}(m_b^{\overline{MS}}) = 4.18(3). \tag{2.64}$$

# Chapter 3

# Data, Analysis, and Results

This chapter pulls together the methods of §2.4 to calculate $r_0\Lambda_{(0)}^{\overline{MS}}$ and $r_0\Lambda_{(2)}^{\overline{MS}}$. Equipped with these values, the methods of §2.5 are used to cross the strange, charm, and beauty thresholds, finally determining $\alpha_{\overline{MS}}^{(n_f=5)}(m_Z)$.

## 3.1 $n_f = 0$

The quenched data for $\beta$, $r_0/a$, and $P$ shown in Table 3.1 is taken directly from [10]. The $r_0\Lambda_{(0)}^{\overline{MS}}$ $\mathrm{I}_0$ values come from Method I in the bare lattice scheme, the $r_0\Lambda_{(0)}^{\overline{MS}}$ $\mathrm{I}_\Box$ values are found using Method I in the boosted coupling scheme, and the $r_0\Lambda_{(0)}^{\overline{MS}}$ II and $r_0\Lambda_{(0)}^{\overline{MS}}$ IIP values are calculated using Method II in the boosted coupling scheme without and with the Padé approximant estimations of $\beta_3^\Box$, respectively. Method III and IIIP values are not shown because in the quenched approximation there are no fermions on the lattice, so $c_{sw}^\Box = 0$. This takes away the only difference between Method II and Method III, and

| $\beta$ | $r_0/a$ | $P$ | $r_0\Lambda_{(0)}^{\overline{MS}}$ $\mathrm{I}_0$ | $r_0\Lambda_{(0)}^{\overline{MS}}$ $\mathrm{I}_\Box$ | $r_0\Lambda_{(0)}^{\overline{MS}}$ II | $r_0\Lambda_{(0)}^{\overline{MS}}$ IIP |
|---|---|---|---|---|---|---|
| 5.70† | 2.922(09) | 0.549195(25) | 0.3309(10) | 0.4849(15) | 0.4950(15) | 0.4877(15) |
| 5.80† | 3.673(05) | 0.567651(21) | 0.3708(05) | 0.5106(07) | 0.5200(07) | 0.5130(07) |
| 5.95 | 4.898(12) | 0.588066(20) | 0.4161(10) | 0.5429(13) | 0.5514(14) | 0.5448(13) |
| 6.00 | 5.368(33) | 0.593679(08) | 0.4306(26) | 0.5548(34) | 0.5631(35) | 0.5566(34) |
| 6.07 | 6.033(17) | 0.601099(18) | 0.4464(13) | 0.5666(16) | 0.5746(16) | 0.5683(16) |
| 6.20 | 7.380(26) | 0.613633(02) | 0.4702(17) | 0.5833(21) | 0.5907(21) | 0.5847(21) |
| 6.40 | 9.740(50) | 0.630633(04) | 0.4929(25) | 0.5953(31) | 0.6018(31) | 0.5963(31) |
| 6.57 | 12.18(10) | 0.643524(15) | 0.5066(42) | 0.6010(49) | 0.6069(50) | 0.6018(49) |
| 6.69 | 14.20(12) | 0.651936(15) | 0.5143(43) | 0.6035(51) | 0.6090(51) | 0.6042(51) |
| 6.81 | 16.54(12) | 0.659877(13) | 0.5216(38) | 0.6062(44) | 0.6113(44) | 0.6068(44) |
| 6.92 | 19.13(15) | 0.666721(12) | 0.5313(42) | 0.6128(48) | 0.6177(48) | 0.6133(48) |
| $\infty$ | $\infty$ | 1 | 0.5351(26) | 0.6138(19) | 0.6194(19) | 0.6145(19) |

Table 3.1: Plaquette and $r_0/a$ data for $n_f = 0$, with corresponding $r_0\Lambda_{(0)}^{\overline{MS}}$ values determined using the 4 methods. The last row represents extrapolated values in the continuum limit. Rows containing $\beta$-values marked with a '†' are not used in the fit.

thus the Method III values for $r_0\Lambda_{(0)}^{\overline{MS}}$ are the same as in Method II.

The lattice simulations use the $\mathcal{O}(a)$-improved clover action, so it is expected that the leading order discretization effects should behave like $a^2$. This motivates the extrapolation to the continuum limit with the independent variable being quadratic in the lattice spacing. However, as first discussed in §2.4.1, Figure 3.1a shows that the extrapolation to the continuum limit for $r_0\Lambda_{(0)}^{\overline{MS}}$ is nonlinear in the squared lattice spacing $(a/r_0)^2$ when using the bare lattice scheme. This implies that the discretization errors are not fully controlled in the bare lattice scheme, and that the bare lattice scheme should be abandoned in favour of a scheme that has better control over the discretization effects.

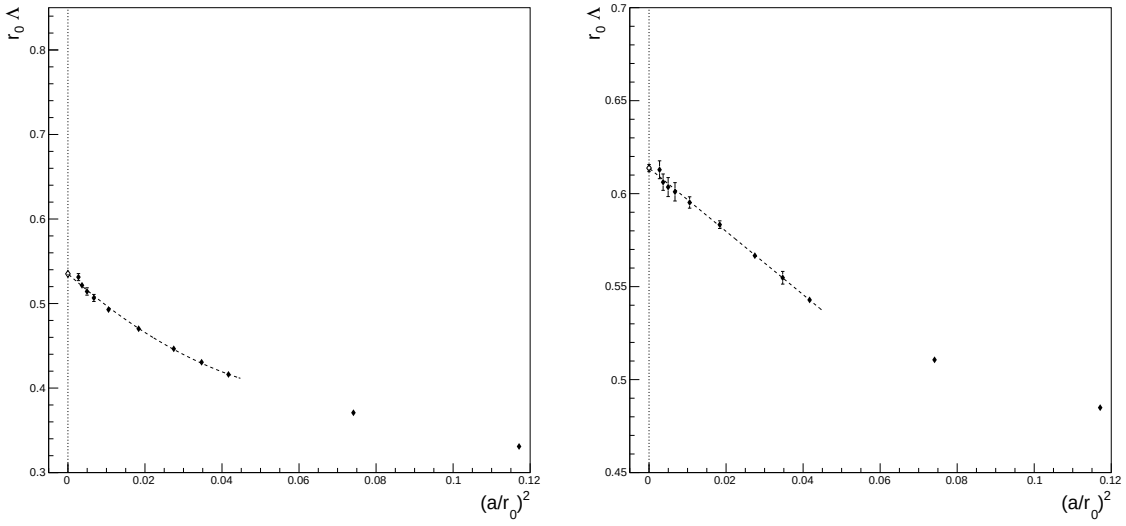


(a) Method $\mathrm{I}_0$ (b) Method $\mathrm{I}_\Box$

Figure 3.1: Extrapolation of $r_0\Lambda_{(0)}^{\overline{MS}}$ to the continuum limit in the quenched approximation for Method I using the bare lattice scheme (left) and the boosted coupling scheme (right).

Figure 3.1b shows that the boosted coupling scheme behaves linearly in the squared lattice spacing, at least for small values of $a$. Consequently, only the boosted coupling scheme will hereafter be considered. Higher order effects can be seen at larger values of $(a/r_0)^2$, so the continuum limit extrapolation is fit using only those datapoints with $(a/r_0)^2 < 0.06$.

The final result for $r_0\Lambda_{(0)}^{\overline{MS}}$ is calculated by taking the mean of the values for Methods I, II, and IIP. The statistical error is the standard deviation of the mean, and the systematic error is estimated from the spread of the three values, taken to be the sample standard deviation. The quoted value is thus[1]

$$r_0\Lambda_{(0)}^{\overline{MS}} = 0.6159(11)(31). \tag{3.1}$$

which should be compared to the world average $r_0\Lambda_{(0)}^{\overline{MS}} = 0.62(2)$ [13]. Using the value of $r_0$ given by eq. (2.7), and combining the statistical and systematic errors of $r_0$ in quadrature (likewise with $r_0\Lambda_{(2)}^{\overline{MS}}$), the physical value for $\Lambda_{(2)}^{\overline{MS}}$ is found to be

$$\Lambda_{(0)}^{\overline{MS}} = 243(7)\ \mathrm{MeV}. \tag{3.2}$$

[1]The ordering of the errors is (stat)(sys).

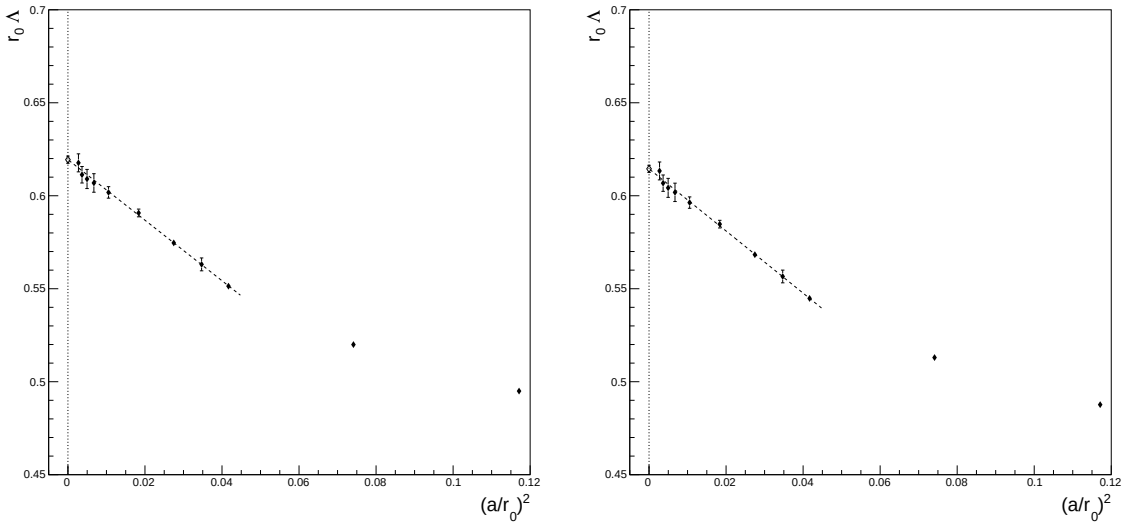


(a) Method II

(b) Method IIP

Figure 3.2: Extrapolation of $r_0\Lambda_{(0)}^{\overline{MS}}$ to the continuum limit with $n_f = 0$ for Method II and Method IIP using the boosted coupling scheme.

## 3.2 $n_f = 2$

Table 3.2 contains the data used for extrapolating $r_0/a$ and $P$ to the chiral limit. The $r_0/a$ data (in the form of $r_0 m_\pi$ and $am_\pi$) is taken from [11], the $\kappa_c$ values are taken from [10], and the plaquette values are taken from a QCDSF-UKQCD private database[2]. The variables $\beta$ and $\kappa$ are put in by hand to the simulation, so the dataset contains multiple reoccurrences of the same values of $\beta$ and $\kappa$ where the sole difference in input is the spatial and temporal extent of the lattice. Wherever these reoccurences appear, the lattice with the largest 4-volume is kept and the others are discarded. Table 3.2 also holds the $r_0/a$ and $P$ values in the chiral limit, extrapolated using the methods described in what follows.

For extrapolating $r_0/a$ to the chiral limit, a global fit is used [10], paramaterized by

$$\ln\left(\frac{r_0}{a}\right) = [a_{0,0} + a_{0,1}\beta] + \left[a_{1,0} + a_{1,1}\beta + a_{1,2}\beta^2\right](am_q) + \left[a_{2,0} + a_{2,1}\beta + a_{2,2}\beta^2\right](am_q)^2 \tag{3.3}$$

where $am_q$ is calculated from $\kappa$ and $\kappa_c$ using eq. (2.3). Despite the lack of data for $r_0/a$ for the smallest value of $\beta$, the global fit is what allows for the determination of $r_0/a$ at $\beta = 5.20$. Figure 3.3 shows this global fit.

The extrapolation of the average plaquette $P$ to the chiral limit is done using a simple quadratic fit in the bare quark mass for each value of $\beta$. Explicitly, the function

$$\frac{r_0}{a} = b_0 + b_1(am_q) + b_2(am_q)^2 \tag{3.4}$$

is fit for each value of $\beta$ in the set $\{5.20,5.25,5.29,5.40\}$. A plot of these fits are shown in Figure 3.4.

[2]D. Pleiter, private communication.

| $\beta$ | $\kappa_c$ | $\kappa$ | Lattice | $r_0/a$ | $P$ |
|---|---|---|---|---|---|
| 5.20 | 0.136008(15) | 0.13420 | $16^3 \times 32$ | - | 0.528994(58) |
| 5.20 | 0.136008(15) | 0.13500 | $16^3 \times 32$ | - | 0.533670(40) |
| 5.20 | 0.136008(15) | 0.13550 | $16^3 \times 32$ | - | 0.536250(30) |
| 5.20 | 0.136008(15) | 0.13565 | $16^3 \times 32$ | - | 0.537070(100) |
| 5.20 | 0.136008(15) | 0.13580 | $16^3 \times 32$ | - | 0.537670(30) |
| 5.20§ | 0.13580 | 0.13580 | - | 6.112(29) | 0.538625(117) |
| 5.25 | 0.136250(07) | 0.13460 | $16^3 \times 32$ | 6.602(56) | 0.538770(41) |
| 5.25 | 0.136250(07) | 0.13520 | $16^3 \times 32$ | 6.603(62) | 0.541150(30) |
| 5.25 | 0.136250(07) | 0.13575 | $24^3 \times 48$ | 6.600(56) | 0.543135(15) |
| 5.25 | 0.136250(07) | 0.13600 | $24^3 \times 48$ | 6.603(65) | 0.544038(09) |
| 5.25 | 0.136250(07) | 0.13620 | $32^3 \times 64$ | 6.600(116) | 0.544782(29) |
| 5.25§ | 0.13620 | 0.13580 | - | 6.593(32) | 0.544930(34) |
| 5.29 | 0.136410(09) | 0.13400 | $16^3 \times 32$ | 7.004(57) | 0.542400(50) |
| 5.29 | 0.136410(09) | 0.13500 | $16^3 \times 32$ | 7.004(59) | 0.545520(29) |
| 5.29† | 0.136410(09) | 0.13550 | $12^3 \times 32$ | 7.004(104) | 0.547293(44) |
| 5.29† | 0.136410(09) | 0.13550 | $16^3 \times 32$ | 7.005(67) | 0.547104(44) |
| 5.29 | 0.136410(09) | 0.13550 | $24^3 \times 48$ | 7.003(57) | 0.547094(23) |
| 5.29† | 0.136410(09) | 0.13590 | $12^3 \times 32$ | 7.005(190) | 0.548569(59) |
| 5.29† | 0.136410(09) | 0.13590 | $16^3 \times 32$ | 7.002(79) | 0.548317(30) |
| 5.29 | 0.136410(09) | 0.13590 | $24^3 \times 48$ | 7.002(56) | 0.548286(57) |
| 5.29 | 0.136410(09) | 0.13620 | $24^3 \times 48$ | 7.004(70) | 0.549187(16) |
| 5.29† | 0.136410(09) | 0.13632 | $24^3 \times 48$ | 7.005(99) | 0.549542(09) |
| 5.29† | 0.136410(09) | 0.13632 | $32^3 \times 64$ | 7.009(73) | 0.549541(08) |
| 5.29 | 0.136410(09) | 0.13632 | $40^3 \times 64$ | 7.000(61) | 0.549540(08) |
| 5.29† | 0.136410(09) | 0.13640 | $40^3 \times 64$ | 7.015(136) | 0.549546(12) |
| 5.29 | 0.136410(09) | 0.13640 | $48^3 \times 64$ | 7.000(136) | 0.549782(06) |
| 5.29§ | 0.13580 | 0.13580 | - | 7.005(34) | 0.549811(19) |
| 5.40 | 0.136690(22) | 0.13500 | $24^3 \times 48$ | 8.285(75) | 0.559000(19) |
| 5.40 | 0.136690(22) | 0.13560 | $24^3 \times 48$ | 8.287(79) | 0.560246(10) |
| 5.40 | 0.136690(22) | 0.13610 | $24^3 \times 48$ | 8.284(81) | 0.561281(08) |
| 5.40 | 0.136690(22) | 0.13625 | $24^3 \times 48$ | 8.286(83) | 0.561550(07) |
| 5.40† | 0.136690(22) | 0.13640 | $24^3 \times 48$ | 8.283(106) | 0.561895(12) |
| 5.40 | 0.136690(22) | 0.13640 | $32^3 \times 64$ | 8.279(84) | 0.561887(10) |
| 5.40† | 0.136690(22) | 0.13660 | $32^3 \times 64$ | 8.284(111) | 0.562278(05) |
| 5.40 | 0.136690(22) | 0.13660 | $48^3 \times 64$ | 8.281(93) | 0.562274(05) |
| 5.40§ | 0.13580 | 0.13580 | - | 8.275(40) | 0.56246(48) |

Table 3.2: The $n_f = 2$ dataset. Rows containing $\beta$-values marked with a '†' are not used in the fit, and rows containing $\beta$-values decorated with a '§' are in the chiral limit.

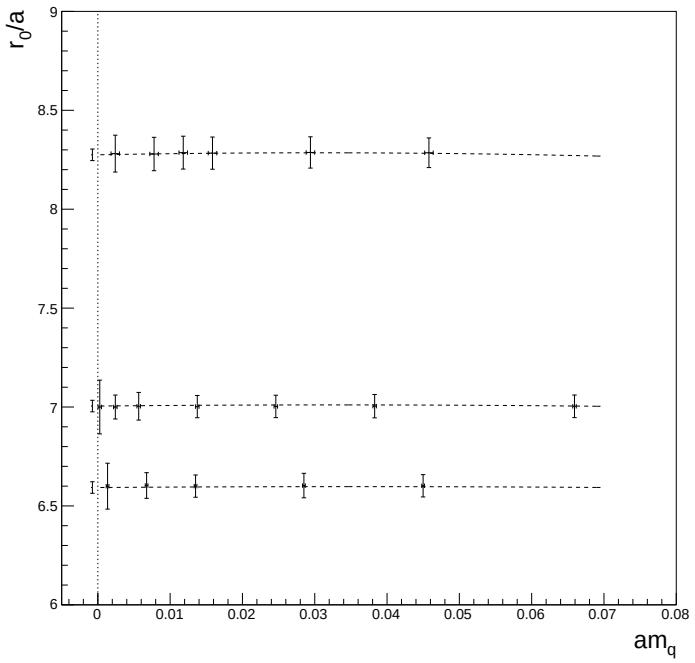


Figure 3.3: Extrapolation of $r_0/a$ to the chiral limit using the global fit hypothesis. Extrapolated points are shifted left for aesthetic purposes.

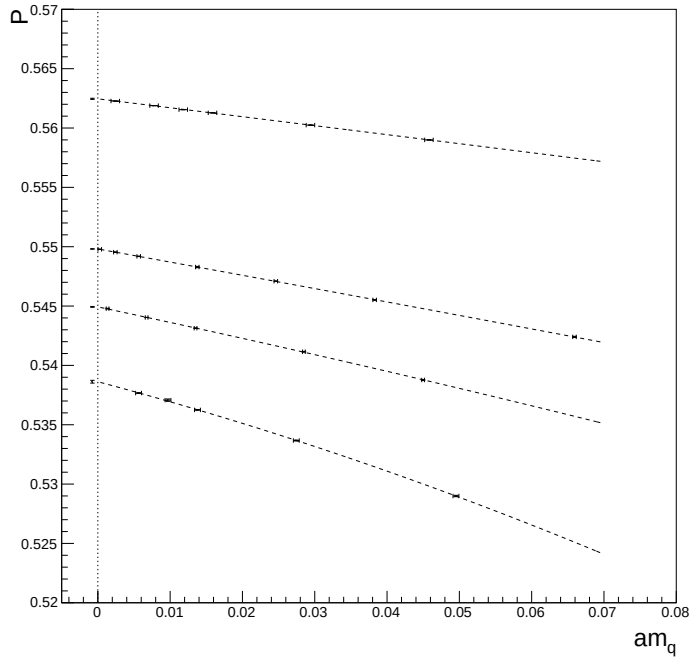


Figure 3.4: Extrapolation of the average plaquette $P$ to the chiral limit. From the bottom, the fitted lines correspond to $\beta = 5.20$, 5.25, 5.29, and 5.40. Extrapolated points are shifted left for aesthetic purposes.

Using the chiral values for $r_0/a$ and $P$ marked with an '§' in Figure 3.2, $r_0\Lambda_{(2)}^{\overline{MS}}$ can now be calculated for each value of the coupling $\beta$ and the continuum limit taken. These $r_0\Lambda_{(2)}^{\overline{MS}}$ values are shown in Table 3.3, calculated using each of the methods introduced in §2.4.

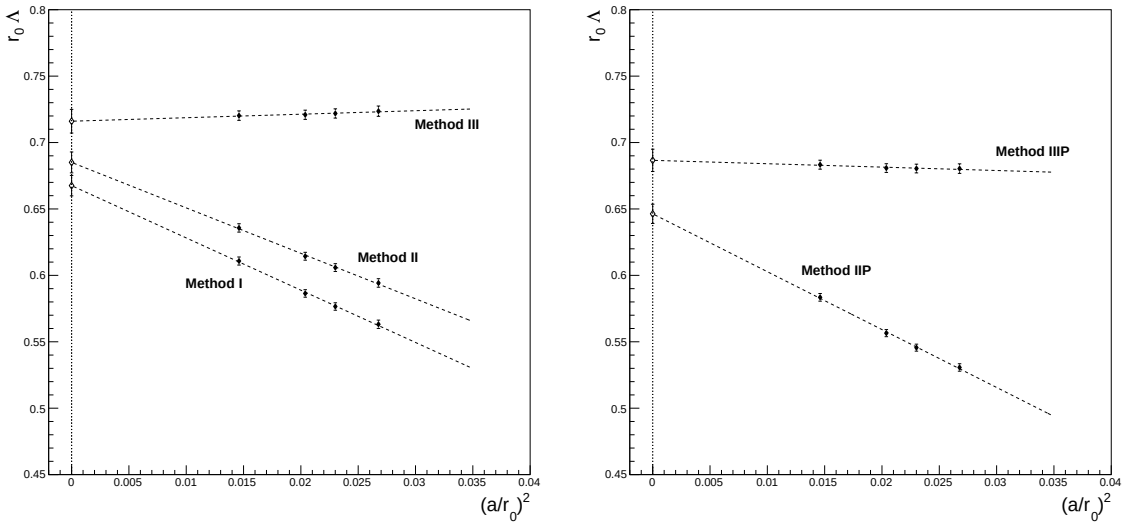


(a) (b)

Figure 3.5: Extrapolation of $r_0\Lambda_{(2)}^{\overline{MS}}$ to the continuum limit with $n_f = 2$ for the three methods (left) as well as the two Padé improved methods (right).

| $\beta$ | $r_0\Lambda_{(2)}^{\overline{MS}}$ I | $r_0\Lambda_{(2)}^{\overline{MS}}$ II | $r_0\Lambda_{(2)}^{\overline{MS}}$ IIP | $r_0\Lambda_{(2)}^{\overline{MS}}$ III | $r_0\Lambda_{(2)}^{\overline{MS}}$ IIIP |
|---|---|---|---|---|---|
| 5.20 | 0.5632(31) | 0.5943(32) | 0.5307(28) | 0.7236(39) | 0.6804(36) |
| 5.25 | 0.5766(28) | 0.6059(29) | 0.5456(26) | 0.7219(35) | 0.6804(33) |
| 5.29 | 0.5864(28) | 0.6144(30) | 0.5565(28) | 0.7209(35) | 0.6808(33) |
| 5.40 | 0.6108(30) | 0.6357(32) | 0.5835(29) | 0.7203(36) | 0.6833(34) |
| $\infty$ | 0.6675(77) | 0.6850(79) | 0.6463(73) | 0.7161(89) | 0.6866(84) |

Table 3.3: The $r_0\Lambda_{(2)}^{\overline{MS}}$ values determined using the three methods plus the two Padé improved methods. The last row shows extrapolated values in the continuum limit.

As in §3.1, the final result for $r_0\Lambda_{(2)}^{\overline{MS}}$ is calculated by taking the mean of the values from Methods I, II, IIP, III, and IIIP. The statistical error is given by the standard deviation of the mean, and the systematic error given by the sample standard deviation. The quoted value for $r_0\Lambda_{(2)}^{\overline{MS}}$, to be compared to the world average $r_0\Lambda_{(2)}^{\overline{MS}} = 0.79(^{+\ 5}_{-13})$ [13], is thus

$$r_0\Lambda_{(2)}^{\overline{MS}} = 0.6803(36)(258). \tag{3.5}$$

The errors affixed to this result show that the statistics for $n_f = 2$ vacuum configurations have reached a level of precision that allow the various methods to be distinguished, whereas this was not the case in [10]. The systematic error drowns out the statistical error,

suggesting that further improvements in simulation technology would be meaningless without first improving the methods used to calculate $r_0\Lambda_{(2)}^{\overline{MS}}$.

Combining the statistical and systematic errors of $r_0$ in quadrature, and likewise in $r_0\Lambda_{(2)}^{\overline{MS}}$, the physical value for $\Lambda_{(2)}^{\overline{MS}}$ is

$$\Lambda_{(2)}^{\overline{MS}} = 268(13)\ \text{MeV}. \tag{3.6}$$

## 3.3 Evolving $\alpha_{\overline{MS}}$ to $m_Z$

Equipped now with physical values for $\Lambda_{(0)}^{\overline{MS}}$ and $\Lambda_{(2)}^{\overline{MS}}$, the methods of §2.5 can be used to find the final result for $\alpha_{\overline{MS}}^{(n_f=5)}$. Beginning by crossing the strange threshold as described in §2.5.1, the value for the ratio $\Lambda_{(2)}^{\overline{MS}}/\Lambda_{(0)}^{\overline{MS}}$ is[3]

$$\frac{\Lambda_{(2)}^{\overline{MS}}}{\Lambda_{(0)}^{\overline{MS}}} = 1.104(43). \tag{3.7}$$

Inputting this value into the matching curves shown in Figure 2.5, the ratio

$$\frac{\Lambda_{(3)}^{\overline{MS}}}{\Lambda_{(2)}^{\overline{MS}}} = 1.068(28)(07) \tag{3.8}$$

is found. The quoted central value is the mean of the values given by considering each of the 1-, 2-, and 3-loop curves in turn. The first error comes from numerically propagating the error from eq. (3.7) through each of the curves then taking the standard deviation of the mean, while the second error comes from the sample standard deviation of the 1-, 2-, and 3-loop $\Lambda_{(3)}^{\overline{MS}}/\Lambda_{(2)}^{\overline{MS}}$ values.

Using the ratio $\Lambda_{(3)}^{\overline{MS}}/\Lambda_{(2)}^{\overline{MS}}$ given in eq. (3.8) and the value for $r_0\Lambda_{(2)}^{\overline{MS}}$ given in eq. (3.5), it is found that

$$\Lambda_{(3)}^{\overline{MS}} = 0.727(32), \tag{3.9}$$

which should be compared to the world average $r_0\Lambda_{(3)}^{\overline{MS}} = 0.81(4)$ [13]. In physical units,

$$\Lambda_{(3)}^{\overline{MS}} = 286(16)\ \text{MeV}, \tag{3.10}$$

whereas the world average is $\Lambda_{(3)}^{\overline{MS}} = 339(17)$ [13]. Again, the statistical and systematic errors of any variable were added in quadrature before propagating through the error.

The remaining thresholds will be crossed using the method of §2.5.2. The quoted errors take into account the error from $\Lambda_{(3)}^{\overline{MS}}$ as well as the errors on the quark masses (see eq. (2.64)). First, the charm threshold is crossed, giving

$$\Lambda_{(4)}^{\overline{MS}} = 244(16)\ \text{MeV}. \tag{3.11}$$

Then the beauty threshold is crossed, resulting in

$$\Lambda_{(5)}^{\overline{MS}} = 172(13)\ \text{MeV}. \tag{3.12}$$

[3]This ratio is calculated directly from the $r_0\Lambda_{(n_f)}^{\overline{MS}}$ values since it is more precise.

Finally, the strong coupling constant $\alpha_{\overline{MS}}^{(n_f=5)}$ is evaluated at the mass of the Z boson, giving the final result

$$\alpha_{\overline{MS}}^{(n_f=5)}(m_Z) = 0.1146(13). \tag{3.13}$$

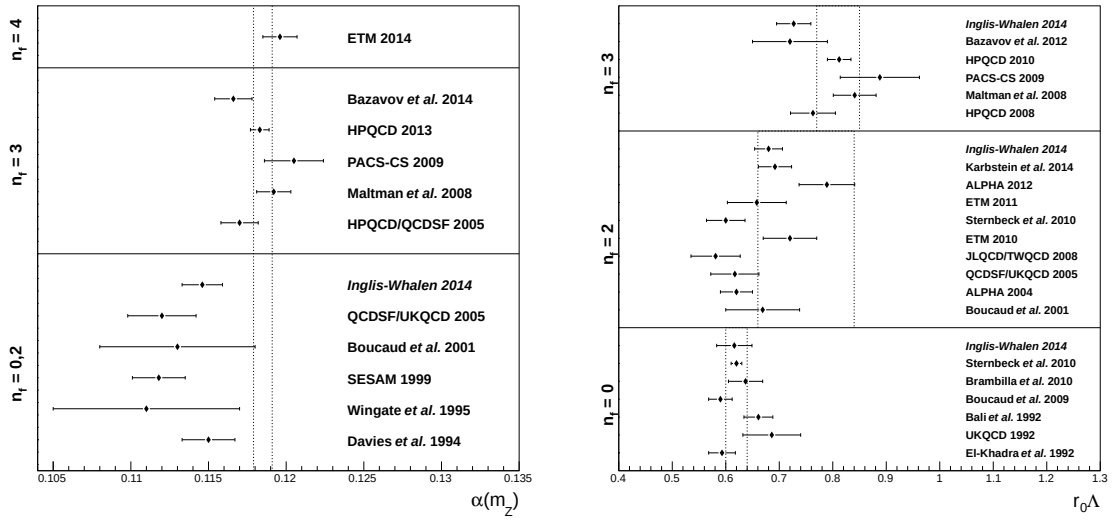


(a) (b)

Figure 3.6: This work's values of $\alpha_{\overline{MS}}^{(n_f=5)}(m_Z)$ (left) and $r_0\Lambda_{(n_f)}^{\overline{MS}}$ (right) compared to other lattice determinations in the literature. The vertical dashed lines represent the 1-$\sigma$ confidence interval for the PDG's (left) and the FLAG Working Group's (right) current world average. Bazavov *et al.* 2014 is taken from [15], Karbstein 2014 is taken from [39], and the remaining values are taken from the FLAG review [13].

Left – Bazavov *et al.* 2014 is taken from [15], with the other values taken from the FLAG review [13].
Right – Karbstein 2014 is taken from [39], with the remaining values taken from the FLAG review [13], which heavily interpreted the original papers. See references therein for more details.

# Chapter 4

# Discussion

This paper closely follows the methods of [10], and as such it was important to replicate the results therein before progressing to the analysis of the newly available data. This goal was achieved, but in the process a few minor differences were found. First, and of negligible numerical difference, was the fact that the four-loop QCD beta function was integrated numerically in [10], whereas in this work the exact form of eq. (2.15) was used. Second, the conversion from the boosted coupling scheme to the $\overline{MS}$ scheme in [10] was done using the reciprocal expansion of eq. (2.28), but in this work the conversion was done using the direct expansion of eq. (2.27). This caused minor differences from the values of $r_0\Lambda_{(0)}^{\overline{MS}}$ shown in Table 3.1, but the continuum limit values agreed within error bars. Third, [10] directly integrated the Padé improved beta function in eq. (2.24), and found a closed form expression for the integral. In contrast, this work continued to use eq. (2.15) as the closed form expression for the integral, using the estimated beta function coefficient $\beta_3^S \approx (\beta_3^S)^2/\beta_1$. Again, this difference caused the calculated $r_0\Lambda_{(2)}^{\overline{MS}}$ values to slightly differ, but the continuum limit values agreed within error bars. Fourth, and perhaps the most interesting difference, is that the matching curves of Figure 2.4 were entirely smooth in [10]. It can be shown analytically that the 1-loop value for $\Lambda_{(2)}/\Lambda_{(0)} \to 1.05144$ as $\alpha_{q\bar{q}} \to \infty$, so the author will remain agnostic as to the methods used by the authors of [10] to generate their matching curves. Finally, the authors of [10] used a simple $\chi^2$ fitting algorithm to determine fitted values and their associated errors. However, the datasets do not contain error free x-values (i.e $(a/r_0)^2$, $am_q$). To properly take these errors into account, the modified variance approach was used[1], which replaces the $\sigma_{y_i}^2$ in the denominator of the $\chi^2$ definition with $\sigma_{y_i}^2 + (\sigma_{x_i} f'(x_i))^2$, where $f'(x_i)$ is the first derivative of the fitted function evaluated at the point $x_i$. This had only a neglible effect on the extrapolated values, but increased their associated errors.

The main motivation for this paper was the new value of $r_0$, as well as the new values for $r_0/a$. The only equation where the new $r_0$ value had any effect on the final result for $\alpha_{\overline{MS}}^{(n_f=5)}(m_Z)$ was eq. (3.10). If the previous value $r_0 = 0.473(33)$fm [10] were to be used, $\Lambda_{(3)}^{\overline{MS}}$ would increase by 6% of the value found in this work. $\Lambda_{(3)}^{\overline{MS}}$ would still not agree with the world average, though it would be pushed to a high enough value for error bars to overlap. This increase $\Lambda_{(3)}^{\overline{MS}}$ would in turn increase the final $\alpha_{\overline{MS}}^{(n_f=5)}(m_Z)$ value, but still not enough to agree with the world average.

[1] Recommended by CERN's ROOT package, see http://root.cern.ch/root/html/TGraph.html#TGraph:Chisquare .

The effects stemming from the new $r_0/a$ values are much more significant. First, the resulting $r_0\Lambda_{(2)}^{\overline{MS}}$ value is much higher than in [10], where it was found that $r_0\Lambda_{(2)}^{\overline{MS}} = 0.617(45)$. This low value was propagated through the matching procedure, giving $r_0\Lambda_{(2)}^{\overline{MS}} = 0.616(35)$, and finally $\alpha_{\overline{MS}}^{(n_f=5)} = 0.1120(22)$. The new $r_0/a$ values were crucial to boosting up the $r_0\Lambda_{(2)}^{\overline{MS}}$ in the chiral limit so that they could reach a value of $r_0\Lambda_{(2)}^{\overline{MS}}$ in the continuum limit that agreed with the FLAG world average.

Secondly, and unexpectedly, the new $r_0/a$ data produced a significantly cleaner global fit extrapolation to the chiral limit for the $r_0/a$ values themselves (see Figure 3.3). In [10], each of the $a_{i,j}$ fit parameters of eq. (3.3) were needed to properly fit the data. In this work, however, the $r_0/a$ values were almost perfectly independent of the bare quark mass. As a result, if the parameters $a_{1,j}$ and $a_{2,j}$ are fixed to zero, the extrapolated $r_0/a$ values in the chiral limit change by less 0.1%. This difference is completely obscured by the statistical noise.

Returning to the three methods of §2.4, it is interesting to see the effect that the choice of scale has on the continuum limit value for $r_0\Lambda_{(0)}^{\overline{MS}}$ (see Figures 2.2 and 2.3). It would appear that any value of $r_0\Lambda_{(0)}^{\overline{MS}}$ could be found given the right scale. Yet the chosen scales are somehow unique, knowing now that they correctly reproduce the world average value of $r_0\Lambda_{(0)}^{\overline{MS}}$. As explained in §2.4.1, the region where the slope is smallest is a good choice for $\mu$, but there is no reason to believe that it is the *best* value for $\mu$. In hindsight, it would have also been interesting to plot similar stability curves for $r_0\Lambda_{(2)}^{\overline{MS}}$ in the continuum limit.

Still, it is reassuring to see that the values of $r_0\Lambda_{(0)}^{\overline{MS}}$ and $r_0\Lambda_{(2)}^{\overline{MS}}$ shown in eqs. (3.1) and (3.5) the world average values. This indicates that the methods used to analyze the $n_f = 0$ and $n_f = 2$ datasets work as designed. Unfortunately, this good agreement is not reflected in the value found for $r_0\Lambda_{(3)}^{\overline{MS}}$. Apparently the matching procedure of §2.5.1 did not perform as well as could be hoped.

Yet this appears to be a common theme amongst $n_f = 0$ and $n_f = 2$ lattice calculations. Figure 3.6a shows that when $n_f = 0$ and $n_f = 2$ simulations are used to calculate $\alpha_{\overline{MS}}^{(n_f=5)}(m_Z)$, the resulting values lie systematically below the PDG's current world average. While it is tempting to conclude that the transition into the $n_f = 3$ regime is the uniting stumbling block for these low-$n_f$ lattice studies, it has also been nearly 10 years since $n_f = 2+1$ simulations became available. This has made it unnecessary to cross the strange threshold at all, causing $n_f = 0$ and $n_f = 2$ simulations to fall out of fashion as a tool for calculating $\alpha_{\overline{MS}}^{(n_f=5)}(m_Z)$. One could argue that the advance of computational and theoretical techniques alone is the cause of the gap between the values of $\alpha_{\overline{MS}}^{(n_f=5)}(m_Z)$ determined using $n_f = 0$ and $n_f = 2$ simulations and those values found using $n_f = 2+1$ or $n_f = 2+1+1$ simulations.

Perhaps a more decisive conclusion can be made. Papers continue to be written for the purpose of determining $r_0\Lambda_{(0)}^{\overline{MS}}$ and $r_0\Lambda_{(2)}^{\overline{MS}}$, as shown in Figure 3.6b. Since 2005, the values of $r_0\Lambda_{(0)}^{\overline{MS}}$ have remained mostly constant, but $r_0\Lambda_{(2)}^{\overline{MS}}$ values have been skewed to a higher value by the few most recent data points. This can only be attributed to improved computational and theoretical methods. To see if crossing the strange threshold remains a barrier for calculating $r_0\Lambda_{(3)}^{\overline{MS}}$ using state-of-the-art $r_0\Lambda_{(0)}^{\overline{MS}}$ and $r_0\Lambda_{(2)}^{\overline{MS}}$ values, a crude estimation procedure is employed.

If one takes the central values of the FLAG confidence intervals for $r_0\Lambda^{\overline{MS}}_{(0)}$ (0.62) and $r_0\Lambda^{\overline{MS}}_{(2)}$ (0.75) then use their ratio as input to the matching curves of Figure 2.5, one finds $r_0\Lambda^{\overline{MS}}_{(3)} = 0.85$. This lies at the upper edge of the confidence interval for $r_0\Lambda^{\overline{MS}}_{(3)}$. Converting to a physical value for $\Lambda^{\overline{MS}}_{(3)}$ with the new $r_0$ value of eq. (2.7) and running the coupling constant up to the Z mass, it is found that $\alpha^{(n_f)}_{\overline{MS}}(m_Z) = 0.1181$. This agrees well with PDG's world average.

While this rough estimation is not meant to be conclusive, it convincingly shows that the existing matching procedure used to cross the strange threshold performs as expected for modern $n_f = 0$ and $n_f = 2$ simulations. However, it remains plausible that the $r_0\Lambda^{\overline{MS}}_{(0)}$ and $r_0\Lambda^{\overline{MS}}_{(2)}$ determined in this paper would produce a better result for $\alpha^{(n_f=5)}_{\overline{MS}}(m_Z)$ if a different matching procedure were used to cross the strange threshold.

# Chapter 5

# Conclusions

This work aimed to determine the strong coupling constant $\alpha_{\overline{MS}}^{(n_f=5)}(m_Z)$.

The datasets used in this paper were drawn from the literature. Both $n_f = 0$ and $n_f = 2$ datasets were used. The $n_f = 2$ datasets employed Wilson fermions, non-perturbatively improved with the Sheikholeslami-Wohlert action. To set the scale, a newly determined value of $r_0$ was used, though this pushed results further away from world averages. Updated values of the dimensionless inverse lattice spacing $r_0/a$ were also used, which played a key role in achieving a higher value for $r_0\Lambda_{(2)}^{\overline{MS}}$ in comparison to that found in [10].

Due to the high statistics of the datasets, the three methods (plus the two Pad'e improved methods) could be distinguished from one another. This made the systematic uncertainty larger than the statistical uncertainty for both $r_0\Lambda_{(0)}^{\overline{MS}}$ and $r_0\Lambda_{(2)}^{\overline{MS}}$ in the continuum limit, implying that improving lattice statistics would be fruitless unless accompanied by a similar inprovement in the methodology.

The three methods (plus the two Padé improved methods) resulted in finding the values $r_0\Lambda_{(0)}^{\overline{MS}} = 0.6159(11)(31)$ and $r_0\Lambda_{(2)}^{\overline{MS}} = 0.6803(36)(258)$. Both of these values agreed with the FLAG world averages.

The matching procedure across the strange threshold involved assuming an $n_f$-independent static quark force. Due to the break down of perturbation theory at the measured value of $\Lambda_{(2)}^{\overline{MS}}/\Lambda_{(0)}^{\overline{MS}}$, the procedure required an extrapolation past the point where $\alpha_{q\bar{q}} \to \infty$. This gave the result $r_0\Lambda_{(3)}^{\overline{MS}} = 0.727(32)$. This did not agree with the FLAG world average, but it was argued that this might not represent a failure in the matching procedure.

The strong coupling constant was run up to the scale of the Z mass, and was found to be $\alpha_{\overline{MS}}^{(n_f=5)}(m_Z) = 0.1146(13)$. This did not agree with the PDG world average.

# Appendix A

# Stability Analysis Details

This section briefly outlines the equations used to find $r_0\Lambda_{(0)}^{\overline{MS}}$ as a function of the ratio of scales, as shown in Figures 2.2 and 2.3. Considering first Method I, let $R \equiv \mu/\mu_{\text{I}}$. This implies, from eq. (2.42), that

$$\mu = \frac{R}{a}\exp\left(\frac{t_1^{\square}}{2\beta_0}\right). \tag{A.1}$$

Inserting this into eq. (2.38),

$$\begin{aligned} d_1^{\square} &= -2\beta_0 \ln R \\ d_2^{\square} &= t_2^{\square} - \frac{\beta_1}{\beta_0}t_1^{\square} - 2\beta_1 \ln R + 4\beta_0^2 \ln^2 R. \end{aligned} \tag{A.2}$$

Using these $d_i$ coefficients, $\alpha_{\square}$ is converted to $\alpha_{\overline{MS}}$, and inserted into the central equation

$$r_0\Lambda_{(0)}^{\overline{MS}}(R) = R\left(\frac{r_0}{a}\right)\exp\left(\frac{t_1^{\square}}{2\beta_0}\right)\frac{1}{M_{(0)}^{\overline{MS}}\left(\alpha_{\overline{MS}}(R)\right)}. \tag{A.3}$$

To plot $r_0\Lambda_{(0)}^{\overline{MS}}(R)$ in the continuum limit, the same steps are followed as in §2.4.1, except repeated for each value $R$ that is needed to make a smooth plot.

The process is the same for method I, except now *all* the $d_i^{\square}$ coefficients vanish for $R = 1$. So with $r \equiv \mu/\mu_{\text{II}}$, the scale is set to

$$\mu = \frac{R}{a}\exp\left(\frac{t_1^{\square}}{2\beta_0}\right)\frac{M^{\overline{MS}}\left(\alpha_{\square}(a)\right)}{M^{\square}(\alpha_{\square}(a))} \tag{A.4}$$

from which the $d_i^{\square}$ coefficients are found to be

$$\begin{aligned} d_1^{\square} &= -2\beta_0 \ln R \\ d_2^{\square} &= -2\beta_1 \ln R + 4\beta_0^2 \ln^2 R. \end{aligned} \tag{A.5}$$

The central equation is then

$$r_0\Lambda_{(0)}^{\overline{MS}}(R) = R\left(\frac{r_0}{a}\right)\exp\left(\frac{t_1^{\square}}{2\beta_0}\right)\frac{M^{\overline{MS}}\left(\alpha_{\square}(a)\right)}{M^{\square}(\alpha_{\square}(a))M^{\overline{MS}}\left(\alpha_{\overline{MS}}(R)\right)}. \tag{A.6}$$

Then as before, the same steps are followed as in §2.4.2 to extrpolate to the continuum limit, but for each value of $R$ required to make a smooth graph.

# Bibliography


[1] J. Beringer *et al.* (Particle Data Group), Phys. Rev. D86, 010001 (2012)

[2] K. G. Wilson, Phys. Rev. D **10** (1974) 2445.

[3] S. Durr, Z. Fodor, J. Frison, C. Hoelbling, R. Hoffmann, S. D. Katz, S. Krieg and T. Kurth *et al.*, Science **322** (2008) 1224 [arXiv:0906.3599 [hep-lat]].

[4] I. F. Allison *et al.* [HPQCD and Fermilab Lattice and UKQCD Collaborations], Phys. Rev. Lett. **94** (2005) 172001 [hep-lat/0411027].

[5] A. Abulencia *et al.* [CDF Collaboration], Phys. Rev. Lett. **96** (2006) 082002 [hep-ex/0505076].

[6] U. Van Kolck, L. J. Abu-Raddad and D. M. Cardamone, nucl-th/0205058.

[7] S. Booth *et al.* [QCDSF-UKQCD Collaboration], Phys. Lett. B **519** (2001) 229 [hep-lat/0103023].

[8] S. Booth, M. Gockeler, R. Horsley, A. C. Irving, B. Joo, S. Pickles, D. Pleiter and P. E. L. Rakow *et al.*, Nucl. Phys. Proc. Suppl. **106** (2002) 308 [hep-lat/0111006].

[9] M. Gockeler *et al.* [QCDSF and UKQCD Collaborations], Nucl. Phys. Proc. Suppl. **140** (2005) 228 [hep-lat/0409166].

[10] M. Gockeler, R. Horsley, A. C. Irving, D. Pleiter, P. E. L. Rakow, G. Schierholz and H. Stuben, Phys. Rev. D **73** (2006) 014513 [hep-ph/0502212].

[11] G. S. Bali, P. C. Bruns, S. Collins, M. Deka, B. Glasle, M. Gockeler, L. Greil and T. R. Hemmert *et al.*, Nucl. Phys. B **866** (2013) 1 [arXiv:1206.7034 [hep-lat]].

[12] B. Leder *et al.* [ALPHA Collaboration], PoS LATTICE **2010** (2010) 233 [arXiv:1012.1141 [hep-lat]].

[13] S. Aoki, Y. Aoki, C. Bernard, T. Blum, G. Colangelo, M. Della Morte, S. Drr and A. X. El Khadra *et al.*, arXiv:1310.8555 [hep-lat].

[14] C. McNeile, C. T. H. Davies, E. Follana, K. Hornbostel and G. P. Lepage, Phys. Rev. D **82** (2010) 034512 [arXiv:1004.4285 [hep-lat]].

[15] A. Bazavov, N. Brambilla, X. G. i. Tormo, P. Petreczky, J. Soto and A. Vairo, arXiv:1407.8437 [hep-ph].

[16] B. Blossier, P. Boucaud, M. Brinet, F. De Soto, X. Du, M. Gravina, V. Morenas and O. Pene *et al.*, Phys. Rev. D **85** (2012) 034503 [arXiv:1110.5829 [hep-lat]].

[17] B. Blossier *et al.* [ETM Collaboration], Phys. Rev. D **89** (2014) 014507 [arXiv:1310.3763 [hep-ph]].

[18] C. Gattringer and C. B. Lang, "Quantum Chromodynamics on the Lattice: An Introductory Presentation," Heidelberg: Springer, (2010).

[19] M. Luscher, hep-lat/9802029.

[20] B. Sheikholeslami and R. Wohlert, Nucl. Phys. B **259** (1985) 572.

[21] K. Jansen and R. Sommer, Nucl. Phys. Proc. Suppl. **63** (1998) 853 [hep-lat/9709022].

[22] R. Sommer, Nucl. Phys. B **411** (1994) 839 [hep-lat/9310022].

[23] T. van Ritbergen, J. A. M. Vermaseren and S. A. Larin, Phys. Lett. B **400** (1997) 379 [hep-ph/9701390].

[24] M. Czakon, Nucl. Phys. B **710** (2005) 485 [hep-ph/0411261].

[25] E. Monsay and C. Rosenzweig, Phys. Rev. D **23** (1981) 1217

[26] C. Christou, *et al.*, Nucl. Phys. B **525** (1998) 387 [hep-lat/9801007]

[27] W. Van Assche, arXiv:math/0609094

[28] J. L. Walsh, Jour. Approx. Theory **11** (1974) 225

[29] R. Horsley, H. Perlt, P. E. L. Rakow, G. Schierholz and A. Schiller, Phys. Rev. D **78** (2008) 054504 [arXiv:0807.0345 [hep-lat]].

[30] M. Luscher and P. Weisz, Phys. Lett. B **349** (1995) 165 [hep-lat/9502001].

[31] M. Gockeler, R. Horsley, Y. Nakamura, H. Perlt, D. Pleiter, P. E. L. Rakow, A. Schafer and G. Schierholz *et al.*, PoS LATTICE **2010** (2010) 228 [arXiv:1010.1360 [hep-lat]].

[32] A. V. Smirnov, V. A. Smirnov and M. Steinhauser, PoS RADCOR **2009** (2010) 075 [arXiv:1001.2668 [hep-ph]].

[33] M. Peter, Nucl. Phys. B **501** (1997) 471 [hep-ph/9702245].

[34] Y. Schroder, Phys. Lett. B **447** (1999) 321 [hep-ph/9812205].

[35] Y. Schroder, Nucl. Phys. Proc. Suppl. **86** (2000) 525 [hep-ph/9909520].

[36] S. Necco and R. Sommer, Nucl. Phys. B **622** (2002) 328 [hep-lat/0108008].

[37] K. G. Chetyrkin, B. A. Kniehl and M. Steinhauser, Nucl. Phys. B **510** (1998) 61 [hep-ph/9708255].

[38] K. G. Chetyrkin, J. H. Kuhn and M. Steinhauser, Comput. Phys. Commun. **133** (2000) 43 [hep-ph/0004189].

[39] F. Karbstein, A. Peters and M. Wagner, arXiv:1407.7503 [hep-ph].